Water Resources Research

RESEARCH ARTICLE
10.1029/2023WR036887

Rainfall-Runoff Modeling in Rocky Headwater Catchments for the Prediction of Debris Flow Occurrence

Martino Bernard[1], Matteo Barbini[1], Matteo Berti[2], Mauro Boreggio[1], Alessandro Simoni[2], and Carlo Gregoretti[1]

[1]Department of Land Environment Agriculture and Forestry, University of Padova, Viale dell'Universita, Padova, Italy, [2]Department of Biological, Geological and Environmental Sciences, University of Bologna, Bologna, Italy

Key Points:

- Rainfall and flow monitoring stations to study hydrology of 3 bedrock-dominated catchments prone to debris flows in the Dolomites (Italy)
- Runoff measured by a sharp-crested weir near a debris-flow initiation site used to calibrate and test an event-based rainfall-runoff model
- The calibrated model satisfactorily approximates the initial phase of stage hydrographs recorded during storms that triggered debris flows

Correspondence to:
M. Bernard,
martino.bernard@unipd.it

Citation:
Bernard, M., Barbini, M., Berti, M., Boreggio, M., Simoni, A., & Gregoretti, C. (2025). Rainfall-runoff modeling in rocky headwater catchments for the prediction of debris flow occurrence. *Water Resources Research*, *61*, e2023WR036887. https://doi.org/10.1029/2023WR036887

Received 12 DEC 2023
Accepted 9 DEC 2024

Abstract In the Dolomites, steep rocky cliffs are marked by numerous narrow gullies. When high-intensity short-duration precipitation occurs, these gullies concentrate and direct surface runoff to the screes at the foot of rock cliffs. Surface runoff mixes with loose sediments, creating a solid-liquid surge that, as it moves downhill, increases its volume entraining debris material and transforms into a granular debris flow. Given the ongoing challenge of modeling the relationship between intense rainfall, surface runoff, and debris flow initiation, we take advantage of data from three monitoring stations operating in distinct debris flow active catchments in our study area to make progress. These stations, strategically positioned close to debris flows initiation zones, record videos and different types of flow-stage data, helping us pinpoint the timing and form of incoming discharge hydrographs. Over a 15-year period of observation, we collected a comprehensive data set on runoff and mass movement in these catchments, offering valuable insights into their hydrological behavior and the initiation of granular debris flows. To compute infiltration excess runoff generation, we refined an already existing hydrological model and calibrated it using discharge measured at one of the monitoring stations. Testing this updated model against observations from two other larger debris flow sites showed that it can reproduce the initial phases of a debris flow, when sediment concentration rapidly rises. These findings suggest that a well-tuned hydrological model can predict the discharge from intense, short rainfall events that typically trigger debris flows, as well as the early stages of these phenomena.

Plain Language Summary In the Dolomites (Eastern Italian Alps), during summer thunderstorms, narrow gullies on steep rocky cliffs channel water to loose sediments at the foot of the cliffs. Water mixed with loose debris creates a powerful solid-liquid surge that, moving downhill, turns into a debris flow. Predicting debris flows is challenging due to the complex relationship between heavy rain, water discharge, and sediment movement. However, it is crucial because many human infrastructures are built on debris flow fans. To understand the triggering of debris flows, we used data from three monitoring stations installed in areas where debris flows often start. These stations include various instruments that record videos and different types of water flow data. The significant amount of data recorded over 15 years concerning surface discharge and the initiation of debris flows enabled us to test, refine and calibrate an existing model designed to simulate these processes. Testing this model with data from two other sites showed it could predict the early stages of a debris flow, reproducing the shape and timing when the flow increases quickly. This suggests that a well-calibrated model can forecast both water runoff from intense short rains and the initial phases of debris flows.

1. Introduction

Debris flows are mixtures of water and sediments that rapidly flow downstream along steep slopes. They are highly dangerous due to their destructive power and their sudden nature. The prediction of such phenomena is challenging and holds significant importance in limiting damages and protecting individuals in threatened areas (Jakob & Hungr, 2005). This aspect increasingly engages with social challenges, given that many villages, tourist resorts, and infrastructures are constructed on or intersect with debris flow fans or channels. The current trend of expanding human activities, especially in remote alpine environments, increases society's vulnerability to these processes, necessitating protective measures to ensure population safety while fostering economic and tourist activities (Fuchs et al., 2007; Musumeci et al., 2021; Thiene et al., 2017). Over recent decades, there has been a notable increase in the frequency of debris flows in the alpine environment, attributed to climate change (Stoffel et al., 2014). Climate change leads to an increase in the frequency and intensity of extreme precipitation events, creating the hydrological conditions necessary for triggering debris flows (Bollschweiler & Stoffel, 2010; Floris

et al., 2010). Climate change is also increasing rockfall activity, producing large quantities of sediment required for the development of solid-liquid flows (Damm & Felderer, 2013; Draebing & Krautblatter, 2019; Rengers et al., 2020).

Given the increasing socio-economic impact and frequency of these events, understanding processes involved in debris flow initiation, flow behavior and runout is crucial. Debris flows could be triggered by the erosion of the channel bed through grain-by-grain bulking or the firehose effect (Berti et al., 1999) caused by runoff. This initiation mechanism is the most common in the Dolomites (Eastern Italian Alps), as it occurs in different geological contexts (Coe et al., 2008; Hürlimann et al., 2014; Imaizumi et al., 2006; Kean et al., 2012; Okano et al., 2012). These debris flows are mostly granular because the eroded material mainly consists of boulders, gravel, and sand (Bernard, Boreggio, et al., 2019). Abundant runoff, generated in small and steep headwater catchments after extreme rainfall events, can mobilize channel-bed sediments (Berti & Simoni, 2005; Cannon et al., 2008; Coe & Godt, 2003; Tiranti & Deangeli, 2015). The runoff discharge is thus the principal factor controlling debris flow initiation and magnitude. Sediment and debris supply constitute the other essential requirement and may also limit the overall magnitude of the event (Brayshaw & Hassan, 2009; Theule et al., 2012), although changes in hydroclimatic conditions within the same watershed can modify its dynamics (de Haas et al., 2024).

Most commonly, debris flows in the Dolomites form in response to high-intensity, short-lasting precipitation events (Underwood et al., 2016). Experimental field data have demonstrated that this response is extremely rapid, often occurring within a few tens of minutes (Berti et al., 1999; Kean et al., 2012). Experimental data for small rocky headwater catchments is scarce, typically gathered from channels located downstream of unweathered bedrock (Bouvier et al., 2015; Kean et al., 2012; Moody et al., 2008; Wei et al., 2017), or within forested hillslope areas (Sheridan et al., 2007). The availability of such data sets is crucial for developing appropriate hydrological models. Reliable runoff modeling is of great interest in debris flow risk assessment and mitigation (Hürlimann et al., 2006). Coupled with knowledge of channel morphology and channel bed material properties, it helps in the identification of debris flow initiation areas (Tao & Barros, 2014) and allows for a reliable determination of solid-liquid hydrographs (Lanzoni et al., 2017; Takahashi, 2014), which can be routed downstream by means of numerical models (Barbini et al., 2024; Han et al., 2017; Pudasaini & Mergili, 2019; Rickenmann et al., 2006).

In this paper, we take advantage of experimental field data recorded in three different watersheds of the Dolomites to update, calibrate, and test a hydrological model specifically proposed for small, steep headwater catchments (Gregoretti et al., 2016), with the aim to address the following research questions:

- Can a calibrated hydrological model predict debris flow occurrences?
- If so, can the simulated hydrographs replicate the initial stages of debris flows?

Therefore, the goals to be achieved include providing reliable input hydrographs for the debris flow triggering and propagation modeling chain, and forecasting debris flow events based on rainfall inputs for early warning purposes. It is important to acknowledge that this work does not explicitly address the triggering mechanisms of debris flows, which involve sediment erosion and incorporation within the liquid discharge. Nevertheless, achieving these goals would be highly significant and directly relevant to hazard management, as well as in mitigating the socioeconomic impact of debris flows on inhabited areas and transportation infrastructure.

2. Materials and Methods

2.1. Study Area

The three monitored catchments are located on the left side of the Upper Boite Valley in 15 km distance from each other (map inset in Figure 1). The left side of the Boite Valley is characterized by steep rocky cliffs overhanging scree with a thick surface layer of colluvial material composed mainly of gravel (50%–75%) and sand (22%–50%), with a low percentage of clay and silt (up to 4%) according to grain size analysis carried out on samples from debris flow initiation and deposition areas (Berti et al., 1999; Gregoretti et al., 2018; Simoni et al., 2020). The rocky cliffs are incised by several gullies that typically progress as debris flow channels on the scree at their base. Runoff descending along the cliffs concentrates in these gullies and causes erosion of downstream screes, forming a channel head. The continuous action of runoff and mass movements-related phenomena, mainly runoff-generated debris flows, has led to the formation of debris flow channels, with several of them posing a threat to the national road SS 51 that runs along the valley bottom.

10.1029/2023WR036887

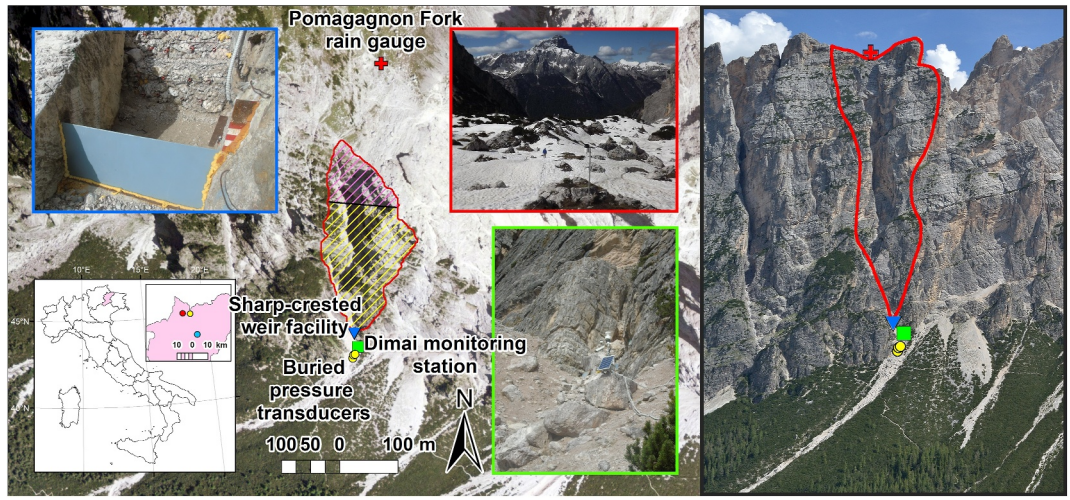

Figure 1. Aerial and frontal views of the Dimai headwater catchment (outlined in red) with measurement facilities. The black line divides the areas of influence of the Dimai monitoring station and the Pomagagnon Fork rain gauge. Inserts show: the sharp-crested weir facility (top left), Pomagagnon Fork rain gauge (top right), and Dimai monitoring station (bottom right). In the bottom left inset, red, yellow, and blue circles mark the Dimai, Rio Gere, and Rovina di Cancia watersheds, respectively.

The rocky massifs in this area are mainly calcareous-dolomitic and belong to the limestones of the "Calcari Grigi" overlaid by the thick dolomitic succession of the "Dolomia Principale" Formation. Due to their chemical composition, these rocky cliffs are characterized by a high degree of fracturing and are susceptible to both strong weathering (Marchi et al., 2008) and large failures (Bernard, Berti, et al., 2019; Gregoretti et al., 2018). More details about the geological setting can be found in Gatter et al. (2018). The geomorphological characteristics of the catchments are summarized in Table 1 and have been computed using high-resolution digital elevation models (DEMs, 1 m grid size) derived from Light Detection and Ranging (LiDAR) surveys conducted on different dates. The use of high-resolution digital topographic data sets is crucial for improving the definition of a catchment compared to using conventional contour lines on maps. In contrast to the findings of Boreggio et al. (2022) regarding the hydraulic propagation of debris flows, Degetto et al. (2015) highlighted the importance of accurately describing the initial surface topography prior to hydrological simulations. Focusing on the Dimai and Rovina di Cancia catchments (Sections 2.1.1 and 2.1.3), they demonstrated how contour-based DEMs can inaccurately determine watershed divides and smooth real surfaces, creating artificial and incorrect flow paths that could significantly influence hydrological simulations.

Table 1
Morphological Characteristics of the Dimai, Rio Gere and Rovina di Cancia Catchments, Extracted From 1 m Resolution DEMs Obtained From LiDAR Surveys Carried Out in 2011 (Dimai), 2015 (Rovina di Cancia), and 2017 (Rio Gere)

	Dimai	Rio Gere	Rovina di Cancia
Latitude (°)	46.5721	46.5618	46.4422
Longitude (°)	12.1334	12.1931	12.2453
Area (km^2)	0.032	0.928	0.654
Min elevation (m a.s.l.)	1,716	1,932	1,662
Mean elevation (m a.s.l.)	2,043	2,500	2,213
Max elevation (m a.s.l.)	2,306	3,220	3,067
Mean slope (°)	72.3	50.6	54.2
Max slope (°)	88.3	89.3	87.8
Channel mean slope (°)	67.2	34.3	36.5
Lidar survey			
Year	2011	2017	2015
Point density (pts/m^2)	3.0	3.8	4.3
Land cover			
Bare rock	95%	70%	50%
Scree and active erosion	–	23%	28%
Moors and heathland	5%	7%	22%

2.1.1. Dimai Catchment

The Dimai watershed (Cortina d'Ampezzo, Figure 1) has an area of 0.032 km^2, a mean elevation of 2,043 m a.s.l., and an average slope of 72.3°. It is drained by a rocky gully incised on the Dimai Peak. The gully is usually dry and the channel bed is characterized by high vertical steps (about 5–10 m), with the presence of several boulders. Its mean slope is 67.2°. The gully ends on a scree that is not deeply incised because of the presence of giant rocks that retain sediments and prevent large excavations. Downstream of it, there is the head of a debris flow channel, on whose left bank the monitoring station is located.

2.1.2. Rio Gere Catchment

The catchment of Rio Gere (Figure 2) is located in the municipality of Cortina d'Ampezzo and serves as a tributary of the Bigontina torrent. Bounded by the

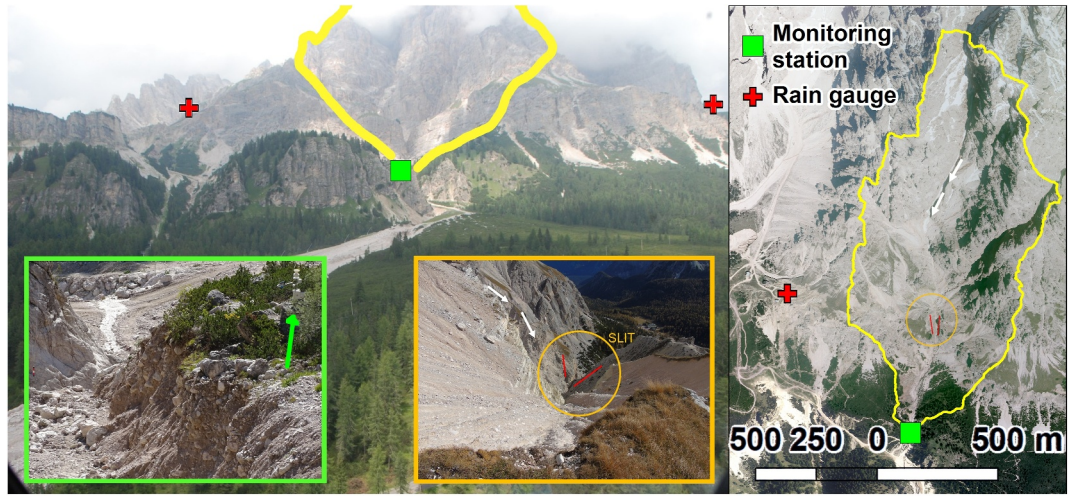

Figure 2. Aerial and frontal views of the Rio Gere watershed. Inserts display the monitoring station and a detail of the channel slit upstream of the monitored section. The green marker indicates the monitoring station location, and the red marker denotes stand-alone rain gauges.

southern slopes of the Cristallo massif, it extends downstream, crossing the regional road SR 48 at 1,675 m a.s.l., just upstream of the confluence with the creek Bigontina. This debris flow catchment has recently been very active (Bernard & Gregoretti, 2021), with the most catastrophic event occurring on 4 August 2017, resulting in one fatality (Baggio et al., 2021). At the base of a gully incised on the cliffs of Cristallo peak, a debris flow channel incises the scree beneath the cliffs. The scree shows a transverse slope from right to left and it is subject to several shallow failures, contributing to the supply of debris material to the right side of the channel. The channel leads to a narrow opening between two rocky cliffs, and downstream of this slit, runs between a rocky cliff on the right and a scree on the left. Just below the slit, two tributaries join the channel: one is a channel incised on the scree, and the other is a gully incised on a rocky cliff. At an elevation of about 1,890 m a.s.l., the debris flow channel exits onto a fan that terminates at the valley bottom. Positioned just upstream of the fan exit is a monitoring station. Additionally, downstream of the narrow opening, there is flowing water within the channel. The hydrological catchment shown in Figure 2, enclosed at the monitoring station, has an area of 0.928 km^2, and an average slope of 50.6°.

2.1.3. Rovina di Cancia Catchment

The catchment of Rovina di Cancia (Figure 3) is located in the municipality of Borca di Cadore, on the left side of the Upper Boite river valley, and is delimited by the western slope of Mount Antelao. It originates at Salvella Fork (2,451 m a.s.l.) and develops downstream, joining with the Bus del Diau tributary on the left at 1,320 m a.s.l. and reaching Borca di Cadore, situated at 940 m a.s.l. Finally, it joins the Boite river at 880 m a.s.l. In the past, this catchment has experienced several debris flows, as documented in the literature (Bacchini & Zannoni, 2003; Simoni et al., 2020). At the base of Salvella Fork, there is a scree incised by a channel. In the upper part of the channel, several large rocks (up to 4–5 m in diameter) are present, which prevent the accumulation of sufficient debris deposits for the formation of debris flows. However, upstream of a giant rock located at 1,666 m a.s.l. in front of the monitoring station (lower left inset in Figure 3), significant quantities of sediment can accumulate, leading to the formation of consistent deposits. Depending on the condition of these deposits, debris flows can initiate either upstream or downstream of the giant rock. After significant debris flow events, the deposit empties, as was the case in 2015, and debris flows form downstream of the giant rock (Simoni et al., 2020). At this point, on the left bank of the channel, a monitoring station is located. The watershed enclosed at the monitoring station has an area of 0.654 km^2, and an average slope of 54.2°.

2.2. Monitoring Stations

Each monitoring station is equipped with various sensors. Each of them includes a rain gauge and multiple video cameras, all controlled by a programmable data logger. The stations are powered by batteries that are recharged by

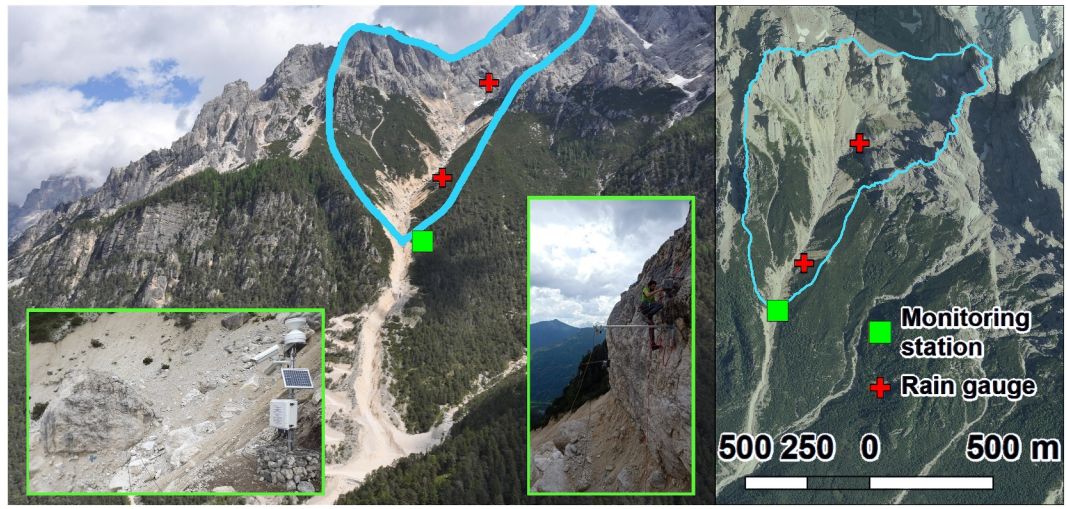

Figure 3. Aerial and frontal views of the Rovina di Cancia catchment. Inserts show the monitoring station and the setup of laser and radar distance meters over the channel. The green marker indicates the monitoring station, while the red marker denotes the stand-alone rain gauge.

solar panels, and data are recorded at 5-min intervals in normal mode. When the cumulative rainfall exceeds the threshold of 0.6 mm in 2.5 min, the data acquisition mode switches to alarm mode, and the video cameras are activated. In alarm mode, recording lasts for 1.5 or 2 hr, and the acquisition interval shifts to 1 or 5 s, depending on the hardware characteristics of the station. If the rainfall intensity remains above the threshold at the end of the recording period, the alarm mode continues for another 1.5 or 2 hr. The threshold is set based on field experience and not on previous works (such as Zimmermann et al. (1997)) because it should be low enough to not miss the recording of events but not too low to avoid filling the memory of the data logger. The monitoring stations allow for the observation of runoff at the outlet of a rocky gully and on the scree below it, in close proximity to the origin of the debris flow channel (Dimai). In addition, they provide data on both runoff and the initial phases of debris flow formation and routing at two sites well downstream from the head of a debris flow channel (Rio Gere and Rovina di Cancia). The monitoring stations operate from May or June until October, depending on the timing of snowpack melting and formation, respectively.

2.2.1. Dimai Station

In early July 2010, a monitoring station was installed at the base of Dimai Peak (green square in Figure 1). It was equipped with a rain gauge, three pressure transducers buried into the scree downstream the rocky gully descending from Dimai Peak (yellow circles in Figure 1), and two video cameras pointing to the gully outlet and to scree. The two cameras record images on an internal disk at a frequency of 125 Hz. Furthermore, at the outlet of the rocky gully, a small watershed ending with a sharp-crested weir was installed and equipped with a pressure transducer in August 2011 (blue triangle in Figure 1), permitting the measurement of the surface discharge descending along the gully. A time-lapse camera (Brinno TLC200) monitors the catchment and records the images on an SD card, capturing a frame every 30 s. To complete the spatial distribution of the precipitations fallen in the catchment, a stand-alone tipping bucket rain gauge has been placed upstream the watershed, on the Pomagagnon Fork (2,180 m a.s.l) (red marker in Figure 1). In this way, it is possible to subdivide the catchment area by using Thiessen polygons in two sub-areas of influence, each of those referring to a different rain gauge. For more details about both the monitoring station and the evaluation of discharges, refer to Bernard (2018). At the end of 2017, the Dimai monitoring station was dismissed because a huge rockfall completely destroyed the sharp-crested weir facility.

Between 2010 and 2017, approximately 220 summer precipitation events triggered the alarm mode (data up to 2016 were already analyzed in Berti et al. (2020)). As previously observed by Prenner et al. (2019) in another context but applicable to our monitored area, rainfall events generally exhibit two different patterns: precipitations with low and steady intensity values (long-lasting rainfalls, LLRs), or highly variable rainfalls with the presence of short, high-intensity episodes (short-duration storms, SDSs). The definition of an SDS or burst is not

unambiguous in the literature: Berti and Simoni (2005) considered it as a period of intense rainstorm that exceeds an average value of 0.5 mm/5 min; Gregoretti and Dalla Fontana (2007) defined a burst of rainfall as starting when the intensity exceeds 0.8 mm in 5 min and ending when the intensity drops below this value; Coe et al. (2008) defined it considering gaps between tips in the rain gauge bucket, setting a minimum separation time of 10 min between two consecutive storms. In this work, to separate and define rainfall events, we followed the approach used by Coe et al. (2008). Precipitations have been classified based on their capability to generate liquid or solid-liquid discharge, aiming to understand how the catchment responds to rain forcing. This classification was possible through the analysis of both the pressure transducers (located in the stilling basin and those buried in the downstream scree when the weir was missing, Figure 1) and the recorded videos.

The sharp-crested weir facility permitted the recording of data from July 2010 to August 2011 and from August 2013 to the end of 2017. In this period, approximately 25 significant surface runoff events were observed, and discharge was successfully measured in 17 cases. Measurement of other events failed due to field monitoring issues, such as rockfalls, incorrect positioning of the pressure transducer in the stilling basin, or power shortages in the central unit. Eight events filled the sharp-crested weir facility with boulders and/or sediments (Table 2), rendering the discharge measurements unreliable. Unfortunately, due to the absence of continuous video recording, we cannot distinguish the type of movement and, consequently, cannot determine up to which point the discharge measurements may be considered trustworthy.

2.2.2. Rio Gere Station

The Rio Gere monitoring station was installed in mid-July 2021 on the top of the right bank of the debris flow channel at an elevation of about 1,940 m a.s.l. (green square in Figure 2). It was set up in a section of the channel with a relatively stable channel bed, just downstream of a transversal rocky outcrop, about 150 m upstream of the fan apex. The monitoring system consists of a rain gauge, two CCFC infra-red cameras (frame rate of 7.5 frames/second) and a laser distance meter with 50-Hz sample frequency. The laser distance meter is not hanging over the channel but it is placed on the bank pointing to the channel bottom with an oblique inclination. The presence, and eventually the timing, of discharges has been evaluated through video camera images and/or by the laser meter records. In the area, two stand-alone rain gauges complete the instrumentation (red markers in Figure 2), one of them managed by the Environmental Protection Agency of the Veneto Region.

2.2.3. Rovina di Cancia Station

The monitoring station at Rovina di Cancia (green square in Figure 3) was installed in early July 2014 on the top of the left bank of the debris flow channel in front of a giant rock at 1,666 m a.s.l. (Simoni et al., 2020). It is composed of a rain gauge, two pressure transducers and two Brinno TLC200 cameras that save the images on a SD card, capturing a frame every two seconds. One camera was replaced with a CCFC camera infra-red camera (frame rate of 7.5 frames/second) in 2019. In 2020, both a laser and a radar distance meters were suspended over the channel, just above a pressure transducer, with the aim of measuring the stage of debris flow events. The monitoring installation is completed by two stand-alone tipping bucket rain gauges located at 2,150 m a.s.l. at the feet of the rocky cliffs, and, from summer 2016, at 1,760 m a.s.l. (red markers in Figure 3). The presence of these two rain gauges allows a better observation of the spatial distribution of rainfall across the watershed that could be larger than that recorded by the rain gauges placed in the bottom of the valley (Bernard & Gregoretti, 2021).

2.3. Hydrological Model

The adopted hydrological model has been explicitly developed for dolomitic headwater catchments by Gregoretti et al. (2016). Given the precipitation P, the excess rainfall P_e generating the surface runoff is computed through the CNH method, introduced by Gregoretti et al. (2016). P_e is then routed from each DEM cell (of size Δx) belonging to hillslopes to the channel network along the steepest path assuming a time-invariant velocity U_s that depends on the overpassed land cover types. Finally, surface runoff is routed along the channel to the outlet using the matched diffusivity kinematic-wave model proposed by Orlandini and Rosso (1996).

In the CNH method, P_e is calculated using a simplified Hortonian law when precipitation intensity I is greater than the infiltration rate f_c (assumed constant), as difference between I and f_c; otherwise, it is computed through the Curve Number (CN) method, developed by Soil Conservation Service (1972). CN is a dimensionless parameter that represents the potential of a terrain to generate surface runoff considering the land cover, soil type, and

Table 2
Characteristics of Rainfall Events That Occurred in the Dimai Catchment and Are Linked to Runoff (R) or Mass Movement (MT)

Event	Time	Type	*AMC*	P_5 (mm)	P_2 (mm)	P (mm)	D (min)	I_{MAX} (mm/h)	t_{LC} (min)	C_{PQ}	V_R (10^{-3} m^3)
04 July 2011	21:00	MT	1	7.4	5.8	22.6	40	64.8	–	–	–
18 August 2011	17:55	MT	2	17.8	0.0	16.2	10	98.4	–	–	–
04 August 2013	19:45	MT	1	3.6	3.6	21.4	75	57.6	–	–	–
				2.2	2.2	27.0	80	57.6	–	–	–
				3.3	3.3	22.8	90	48.6	–	–	–
07 June 2015	22:15	MT	2	16.0	15.0	13.8	20	69.6	–	–	–
25 July 2015	18:30	MT	1	12.2	7.0	18.4	30	69.6	–	–	–
				14.2	6.6	17.6	40	57.6	–	–	–
				12.7	6.9	18.2	30	66.6	–	–	–
29 July 2015	17:00	MT	3	30.2	4.6	16.2	35	52.8	–	–	–
				30.6	5.0	15.6	35	64.8	–	–	–
				30.3	4.7	16.1	35	48.6	–	–	–
04 August 2015	17:45	R	3	41.6	0.0	15.8	70	50.4	13	0.58	33.4
				44.0	0.0	13.4	70	40.8	14	0.59	
				42.2	0.0	15.2	70	46.2	13	0.62	
03 September 2015	22:10	R	1	5.0	4.8	13.8	70	31.2	12	0.56	48.9
				5.0	4.8	14.2	70	28.8	17	0.59	
				5.0	4.8	13.9	70	28.2	15	0.58	
13 July 2016	12:40	R	3	41.2	33.4	10.2	55	55.2	11	0.32	26.6
				44.0	29.8	9.2	60	50.4	11	0.31	
				42.2	32.5	10.0	60	50.4	11	0.33	
05 August 2016	07:25	R	2	27.2	3.4	22.6	145	36	17	0.71	55.3
				26.0	4.2	14.8	155	28.8	17	0.61	
				26.9	3.6	20.7	155	31.8	17	0.71	
09 August 2016	16:45	R	3	38.2	2.4	43.0	285	43.2	170	0.22	238.3
				30.4	2.4	39.8	285	43.2	170	0.22	
				36.3	2.4	42.4	285	43.2	170	0.22	
14 August 2016	17:25	MT	3	68.4	1.4	21.0	85	86.4	–	–	–
				65.6	2.8	18.0	80	21.6	–	–	–
				67.7	1.8	18.4	85	68.4	–	–	–
30 May 2017	11:45	R	1	0.0	0.0	31.4	105	84.0	23	0.74	64.3
20 June 2017	20:20	R	1	3.6	3.4	9.6	55	48.0	23	0.21	5.7
21 June 2017	18:55	R	2	13.0	13.0	8.2	30	50.4	5	0.31	5.8
25 June 2017	04:30	R	2	24.4	3.2	20.0	260	9.6	55	0.41	26.9
				33.0	33.0	12.2	250	9.6	55	0.41	
				26.6	5.5	19.3	260	9.6	62	0.42	
28 June 2017	13:50	R	3	36.2	12.6	12.8	115	9.6	28	0.51	18.8
				34.0	13.2	11.6	115	12.0	32	0.56	
				35.7	12.8	12.5	115	10.2	28	0.54	
08 July 2017	19:20	R	1	7.6	4.2	13.6	20	117.6	5	0.4	27.4
				8.4	5.2	7.2	15	60	6	0.36	
				7.8	4.5	12.0	20	103.2	5.0	0.39	
13 July 2017	21:10	MT	2	16.8	0.4	28.2	255	38.4	–	–	–

Table 2
Continued

Event	Time	Type	*AMC*	P_5 (mm)	P_2 (mm)	P (mm)	D (min)	I_{MAX} (mm/h)	t_{LC} (min)	C_{PQ}	V_R (10^{-3} m^3)
				13.6	0.6	28.2	245	50.4	–	–	–
				16.0	0.5	28.2	255	41.4	–	–	–

Note. Events causing runoff prior to 2014 are described in Gregoretti et al. (2016); events up to summer 2016 in Berti et al. (2020). Key terms: *AMC* denotes antecedent moisture conditions; $P_{5/2}$ indicates cumulative rainfall over the past 5/2 days; P denotes the event cumulative rainfall; D represents rainfall duration; I_{MAX} is the peak rainfall intensity over a five-minute period; t_{LC} is the lag time determined by cross-correlation of rainfall and flow discharge timings; C_{PQ} is the cross-correlation coefficient; V_R is the runoff volume. When data from both the Dimai and Pomagagnon Fork rain gauges were available, rainfall data for Dimai, Pomagagnon Fork, and their average are reported.

antecedent moisture conditions (AMCs; dry (I), normal (II), wet (III) conditions). Therefore, for the CNH method, P_e is computed throughout time t as:

$$P_e(t) = \begin{cases} 0 & t \le t_{I_a} \\ \dfrac{(P(t) - I_a)^2}{P(t) - I_a + S} & t > t_{I_a}, I < f_c \\ P_e(t) = P_e(t - \Delta t) + P(t) - P(t - \Delta t) - f_c \Delta t & t > t_{I_a}, I > f_c, P_e < P_{eSCS} \end{cases} \quad (1)$$

Here, t_{I_a} represents the time essential for fulfilling the initial abstraction I_a, that is, the initial rainfall that infiltrates the soil before runoff begins, usually estimated as a fraction of S (the standard assumption reads $I_a = 0.2S$). $S = 25.4[(1000/CN) - 10]$ represents the potential maximum soil moisture retention, I stands for the rainfall intensity during the time step Δt, and P_{eSCS} indicates the excess rainfall computed by the CN method for the rainfall event. Δt is constant and computed as $\Delta t = \Delta x / \max(U_s)$ for respecting the physics of routing. AMC was determined following the instructions by the Soil Conservation Service (1972). When considering the CN values for normal AMC (CN(II)), CN values for dry or wet AMC can be assessed by:

$$CN(AMC) = \frac{aCN(II)}{10 + bCN(II)} \quad (2)$$

where $a = 2.08454e^{0.80709AMC} - 0.47225$, $b = \frac{a-4.2}{100} - 0.058$, and AMC corresponds to dry (I) or wet (III) conditions (Chow et al., 1988).

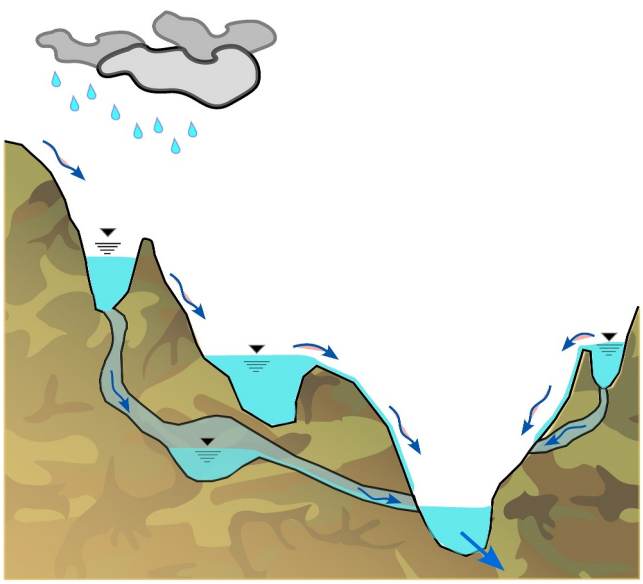

Figure 4. Sketch of an hypothetical cross-section of a dolomitic wall depicting possible mechanisms of precipitation return to the channel.

Essentially, the excess rainfall calculated by the SCS equation represents the contribution of fracture flow, while the excess given by the exceeding of the infiltration rate represents the contribution of direct runoff. In the presence of cliffs with inner fractures and hollows (as occurs in the study area or in similar geological settings), the occurrence of subsurface flow seems unlikely. Instead, fracture flow concentrates along certain paths within fractures and flows out through specific holes (Figure 4). Indeed, water flow spilling out of holes on the cliffs was observed just after the end of rainfall events. To take fracture flow into account, the model has been refined in terms of the methodology for evaluating the parameters to be used in the calculation of effective precipitation, as detailed in the following subsections and Section 3.

As previously mentioned, the model simulates discharge propagation by delineating flow paths based on the steepest descent direction from each DEM cell within the catchment toward the outlet. These paths are subsequently categorized into channel and hillslope flow paths to account for the different propagation velocities associated with each flow regime. This distinction enables the model to represent the impulsive nature observed in discharge hydrographs that trigger debris flows. Hillslope propagation velocity U_s is assumed to be constant and depends on the land cover characteristics. In contrast, channel discharge is routed using the Muskingum-Cunge scheme

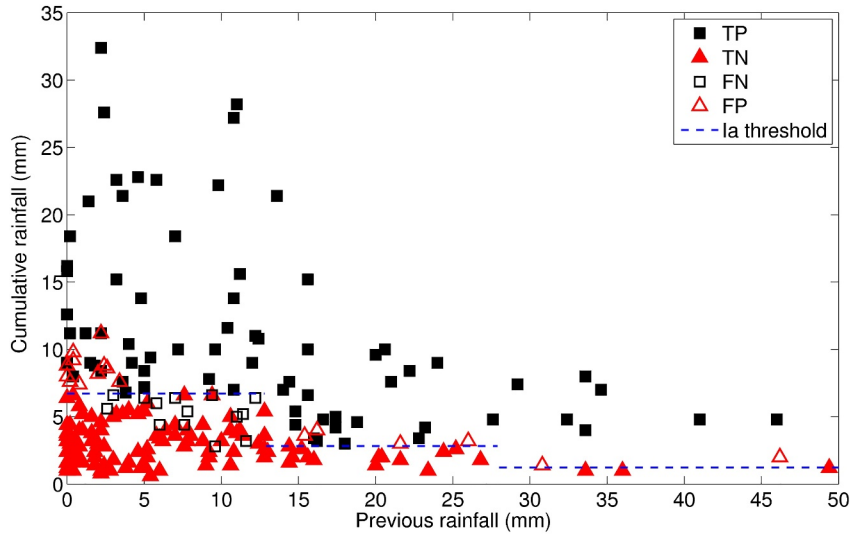

Figure 5. Analyzing runoff prediction by altering *Ia* and AMC parameters, where TP denotes events correctly identified as runoff (true positives) and TN represents events correctly identified as non-runoff (true negatives). FN denotes rainfall events mistakenly not identified as runoff (false negatives), while FP stands for non-runoff events incorrectly identified as runoff (false positives). The *Ia* threshold is adjusted based on AMC values, following the relationship given by Equation 2. The specific case examines the scenario where $Ia = 0.1S$ and AMC is determined using the total rainfall from the preceding 2 days.

proposed by Orlandini and Rosso (1996). This scheme ensures that the numerical diffusion matches the hydraulic diffusivity of the flood wave, leading to an unconditionally stable, grid-size independent, and physically realistic solution. For further details about the equations employed for runoff propagation, refer to Section 4 in Gregoretti et al. (2016).

2.3.1. Setting of CN Parameters

For the modeling of the recorded discharges, defining the appropriate values for the parameters involved—specifically, CN, *Ia*, and Antecedent Moisture Condition (AMC)—is crucial. Due to the interaction between *Ia* and AMC through CN, we performed a sensitivity analysis on the events recorded in the Dimai catchment for choosing the best combination of values to be assigned to the two parameters. We fixed a constant value for the Curve Number $CN = 90$, generally representative of rocky formations and average of CNs found by Gregoretti et al. (2016). We varied the parameter *Ia* within the range of $0.05S$ and $0.2S$, using increments of $0.025S$. Meanwhile, the cumulative prior rainfall, crucial for evaluating AMC, was calculated based on the preceding 1–5 days before the events. After evaluating the various combinations of I_a and AMC for each event, we assessed whether the rainfall exceeded I_a and whether recorded surface runoff was generated in response to the precipitation event. Following this, we evaluated the forecast performance for each I_a-AMC combination using the Critical Success Index (or Threat Score) (Schaefer, 1990; Staley et al., 2013):

$$CSI = \frac{TP}{TP + FP + FN} \tag{3}$$

where *TP* is the number of occurred events positively predicted, *FP* the number of forecasts without occurred events, and *FN* the number of occurred events not predicted (Figure 5). We opted for *CSI* as an indicator because it equally weighs FN and FP errors, without considering a large number of *TN* events, that is, events correctly not forecasted.

2.3.2. Calibration of the f_C Parameter

Calibration of the infiltration rate, denoted as f_C, was performed by fixing the other model parameters to the values established in Gregoretti et al. (2016). The calibration procedure was carried out for the Dimai catchment. These values are related to the propagation velocities along slopes, with U_S set at 0.7 m/s for rocky cliffs and 0.1 m/s for

scree slopes. Additionally, they are related to the Muskingum-Cunge propagation along the rocky channel, where the Gauckler-Strickler friction coefficient is denoted as k_s and set to 9 $m^{1/3}/s$, the catchment outlet width is denoted as $\mathcal{B}_0$ and set at 2 m, and the morphological exponent is denoted as b_1 and set to 0.26. Therefore, the Hortonian infiltration rate, denoted as f_C, becomes the only variable parameter. The events considered in the calibration of the f_C parameter are those that generated a consistent discharge in the stilling basin, such that they can be measured by the pressure transducer. Additionally, events that had incomplete recording or generated solid transport were excluded. These latter events altered the configuration of the facility, making it impossible to correctly assess the inflow runoff in the stilling basin. For each event, the f_C rates were evaluated to best replicate the recorded runoff peak values based on the performance parameter Π_s (Schulz et al., 1999):

$$\Pi_S = 200\,\frac{\sum_{i=1}^{n}|q_{c,i}-q_{o,i}|q_{o,i}}{n\,q_{oMax}^2} \tag{4}$$

where the number of observed discharges is denoted by n, $q_{c,i}$ and $q_{o,i}$ represent the values of computed and observed discharges, respectively, and q_{oMax} signifies the maximum observed discharge value. This parameter is commonly employed to assess the efficacy of hydrological models, with Π_S values typically indicating good performance when falling within the range of 3–10 (Foglia et al., 2009).

Once the f_C parameter was calibrated for every event, we aimed to determine if any relationships with certain variables were present. First, we sought a relation with the AMCs, specifically with the cumulative prior rainfall calculated based on the number of days resulting from the analysis described in Section 2.3.1. To verify the relationship, we simulated the events recorded by the Dimai monitoring station when the weir was missing. The comparison was conducted by evaluating the time difference between the peak of simulated discharges and the arrival of recorded runoff at the monitoring station. Timings were determined using the pressure transducer in the stilling basin, those buried in the screes and/or the video cameras installed at the monitoring station. Given the poor results, especially for the events occurring in wet AMCs, we investigated a different relationship between infiltration and rainfall. Initially, we employed a regression model incorporating various variables related to precipitation characteristics (e.g., duration, cumulative rainfall, intensity) and pre-event cumulative rainfalls of different durations. We simplified the model using a trial-and-error method until the remaining variables were significant for the regressions (with a *p-value* from the Wald test lower than 0.05). The choice to follow a stepwise statistical approach for the selection of significant variables was in accordance with Cannon et al. (2010).

3. Results

3.1. Setting Parameters for Hydrological Modeling

Focusing the attention on the calibration of parameters of the SCS-CN method, especially on the I_a-AMC combination, the best CSI (=72%) was achieved when AMC was calculated based on the total rainfall over the 2 days preceding each event, with an initial abstraction $I_a = 0.1S$, as shown in Table 3.

CN values were calibrated by aligning the volumes of measured and simulated runoff for the events outlined in Table 4 and Figure 6. A substantial variability is observed in the CN range (81.8–92.6), which is influenced by the

Table 3
Values of Critical Success Index (CSI), Determined for Each Combination of Initial Abstraction Ia and AMC by Applying Equation 3

	Ia						
Considered days for AMC assessment	0.050*S*	0.075*S*	0.100*S*	0.125*S*	0.150*S*	0.175*S*	0.200*S*
1 day	0.59	0.66	0.65	0.60	0.48	0.39	0.35
2 days	0.55	0.67	**0.72**	0.67	0.59	0.48	0.43
3 days	0.54	0.62	0.66	0.65	0.61	0.51	0.49
4 days	0.53	0.58	0.61	0.63	0.62	0.56	0.54
5 days	0.51	0.54	0.57	0.58	0.60	0.55	0.55

Note. The best CSI value in bold.

Table 4
Relevant Characteristics of Simulated Runoff Discharges

Event	*AMC*	*CN*	AMC_{NEW}	CN_{NEW}	CN_A	Q_P (l/s)	Q_{CNH-MC} (l/s)	f_C (cm/h)	Π_s
15 August 2011	I	81.3	I	81.3	64.6	0.2	0.1	0.54	
09 August 2013	II	90.6	I	95.6	90.6	10.2	9.6	1.28	4.3/7.2
19 August 2013	I	90.4	I	90.4	79.8	22.4	22.8	2.59	3.7/3.9
24 August 2013	I	83.3	I	83.3	67.7	15.8	15.9	1.76	13.2/13.1
12 August 2014	I	88.4	I	88.4	76.2	15.7	15.7	3.46	4.6/3.7
31 August 2014	I	90.1	I	90.1	79.3	12.9	13.4	1.15	9.8/9.1
04 August 2015	III	62.5	I	90.4	79.8	28.6	31.9	4.46	5.1/7.5
03 September 2015	I	92.8	I	92.8	84.4	34.4	41.1	2.63	6.6/8.3
13 July 2016	III	74	III	74	86.7	28.5	28.1	5	6.4/6.4
05 August 2016	II	76.0	I	88.5	76.0	20.6	22.5	3.38	6.7/10.5
09 August 2016	III	50.3	I	85.7	71.6	38.8	39.7	2.34	8.6/8.6
30 May 2017	I	81.8	I	81.8	65.4	35.7	44.3	7.20	16.9/17.0
20 June 2017	I	90.8	I	90.8	80.6	5.4	5.1	3.42	7.6/7.1
21 June 2017	II	83.9	II	83.9	83.9	13.3	14.1	4.68	5.7/5.9
25 June 2017	II	72.6	I	86.3	72.6	6.5	10.3	0.86	9.9/27.4
28 June 2017	III	63.8	I	90.9	80.7	6.6	8.0	1.12	18.0/62.1
08 July 2017	I	92.2	I	92.2	83.2	43.1	60	2.74	3.9/4.6

Note. Antecedent Moisture Conditions (*AMC*) are determined following the Soil Conservation Service (1972), and Curve Number (*CN*) values of the rocky area, based on AMC. Considering only the rainfall from the previous 2 days, the assessment method recalculates the antecedent moisture conditions (AMC) as AMC_{NEW}. The corresponding absolute CN values for the rocky area are then designated as CN_{NEW}. The CN_{NEW} values are then normalized to CN_A using Equation 2. Peak discharge measurements are represented by Q_P, while Q_{CNH-MC} denotes the peak discharge calculated via the SCS-CNH method coupled with kinematic wave routing with matched diffusivity (Orlandini & Rosso, 1996). The infiltration rate is marked by f_C, and the performance parameter by Schulz et al. (1999) is indicated as Π_s (The first value refers to the hydrographs simulated with the calibrated f_C parameter, the second corresponds to the simulation with the f_C parameter calculated using the relationship in Figure 7c).

antecedent moisture conditions prior to an event: higher AMCs lead to a reduced CN value. The Curve Number absolute values, denoted as CN_A and linked to the AMC of each event, are deduced using Equation 2. These values span from 65.4 to 90.6, averaging at 78.7. Omitting the outliers 71.6 and 72.6, which are associated with two extended rainfalls (longer than 4 hr) on 9 August 2016 and 25 June 2017, the average CN_A stabilizes at 80.2.

Once the CN is set for each considered event, we calibrate the f_C parameter to align the peak discharges of measured and simulated surface runoff, based on the performance parameter Π_s (Equation 4). Π_s resulted in a mean of 8.5, with all but three values lower than 10 (Table 4). It is worth noting that two out of the three worst Π_s values were due to the simulation of longer-duration and lower-intensity rainfalls, specifically the events on the 25th and 28th of June 2017.

When plotting these values against the cumulative rainfall from the preceding 2 days (Figure 7a), nearly all points, except for two, exhibit a trend that closely aligns with a nearly straight line. This alignment indicates a reliance of infiltration on prior rainfall, as suggested by Beven (2002). The events that do not follow this alignment are those that occurred on 13 August 2016, and 21 June 2017. Unlike the other events, they occurred in AMC II and III (depending on whether a 2- or 5-day previous cumulative rainfall is considered). An intriguing observation arises when noting that the linear trend for AMC I events is also reflected in the maximum intensity of certain events that did not generate any runoff (Figure 7b). These events were selected based on the criterion that their maximum rainfall intensity exceeded the infiltration rate f_C, as determined by linear interpolation using the equation shown in Figure 7b.

10.1029/2023WR036887

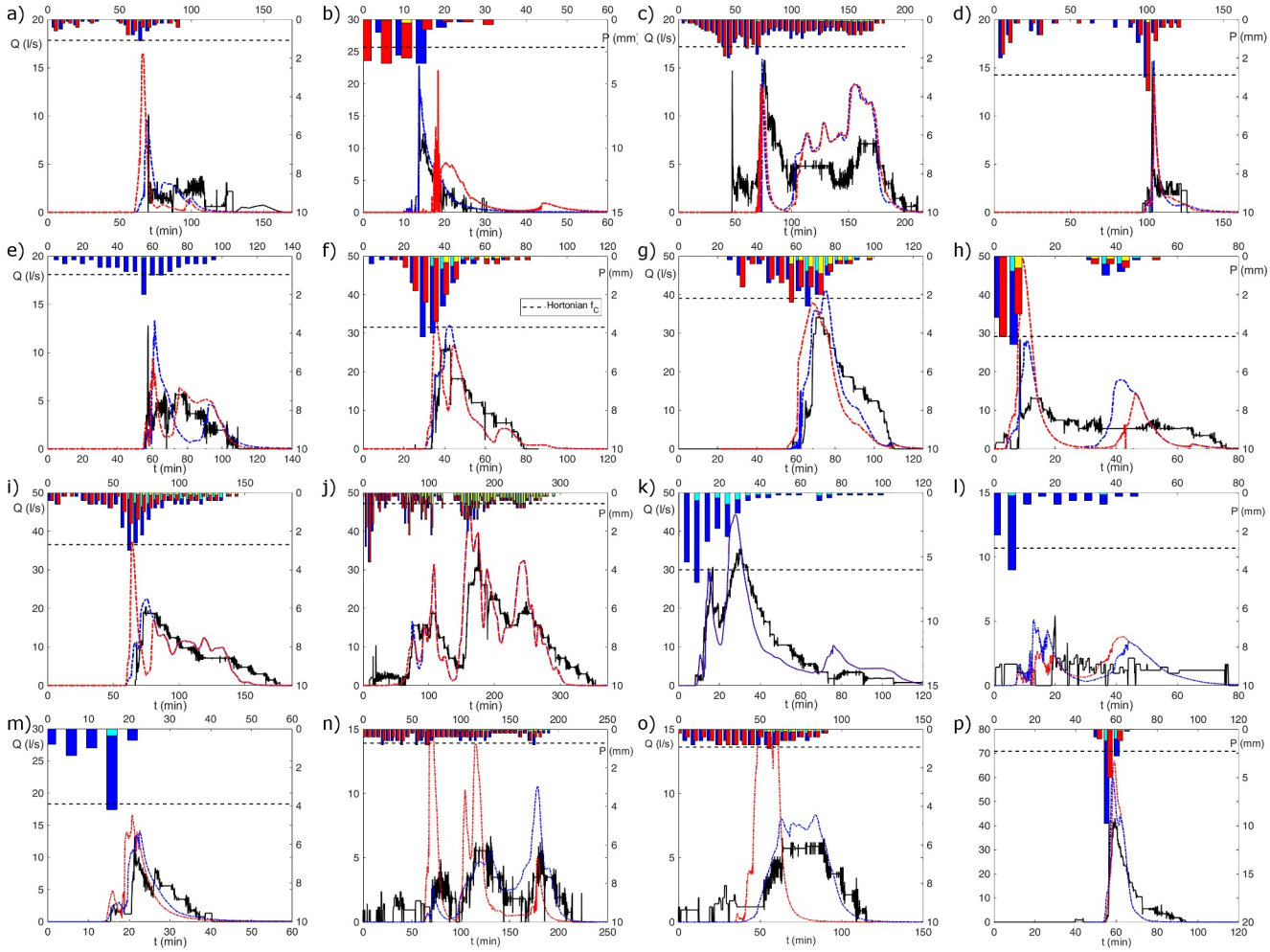

Figure 6. Comparison of runoff discharges: observed values are represented by a continuous line, while simulated values using the SCS-CNH procedure are depicted in red lines for calibrated f_C and in blue lines for f_C assessed by the relationship in Figure 7c. The observed events occurred on: 09 August 2013 (a), 19 August 2013 (b), 24 August 2013 (c), 12 August 2014 (d), 31 August 2014 (e) 04 August 2015 (f), 03 September 2015 (g), 13 July 2016 (h), 05 August 2016 (i), 09 August 2016 (j), 30 May 2017 (k), 20 June 2017 (l), 21 June 2017 (m), 25 June 2017 (n), 28 June 2017 (o), and 08 July 2017 (p). Rainfall and excess rainfall concerning the Pomagagnon Fork rain gauge are depicted in red and yellow, respectively. Meanwhile, blue and cyan depict those relative to the Dimai monitoring station. The timings of rainfalls have been adjusted to align with the centroid of their respective areas of influence (Figure 1).

3.2. Model Testing

We employed the events recorded in the Dimai watershed when the weir was missing to verify the relationship presented in Figure 7b. We simulated the discharge and evaluated the time difference between the peak of the simulated discharges and the arrival of the recorded runoff at the monitoring station. In the simulations, the CN_A coefficient was set to 80.2 in accordance with the findings presented in Section 2.3.1.

The time difference between the recorded and simulated discharges was minimal, with observed events occurring, on average, 0.1 min earlier. This time difference ranged from a 5-min advance to a 6-min delay (see Table 5). For two events in AMC I, we adjusted the predicted infiltration rate to improve the accuracy of the simulated time of occurrence (indicated by empty triangles in Figure 7a). There were only two events with a different AMC. Since the linear relationship shown in Figure 7b does not fully describe the behavior of certain events in AMC I, and does not describe at all the events occurring in higher AMCs, we investigated if any relationship between infiltration and rainfall characteristics exists. In Figure 7c, we present the obtained model. The only significant variable here is the maximum rainfall intensity within 5 min of the events recorded. It suggests that higher precipitation intensity enhances the ability of rainfall to infiltrate in rocky substratum.

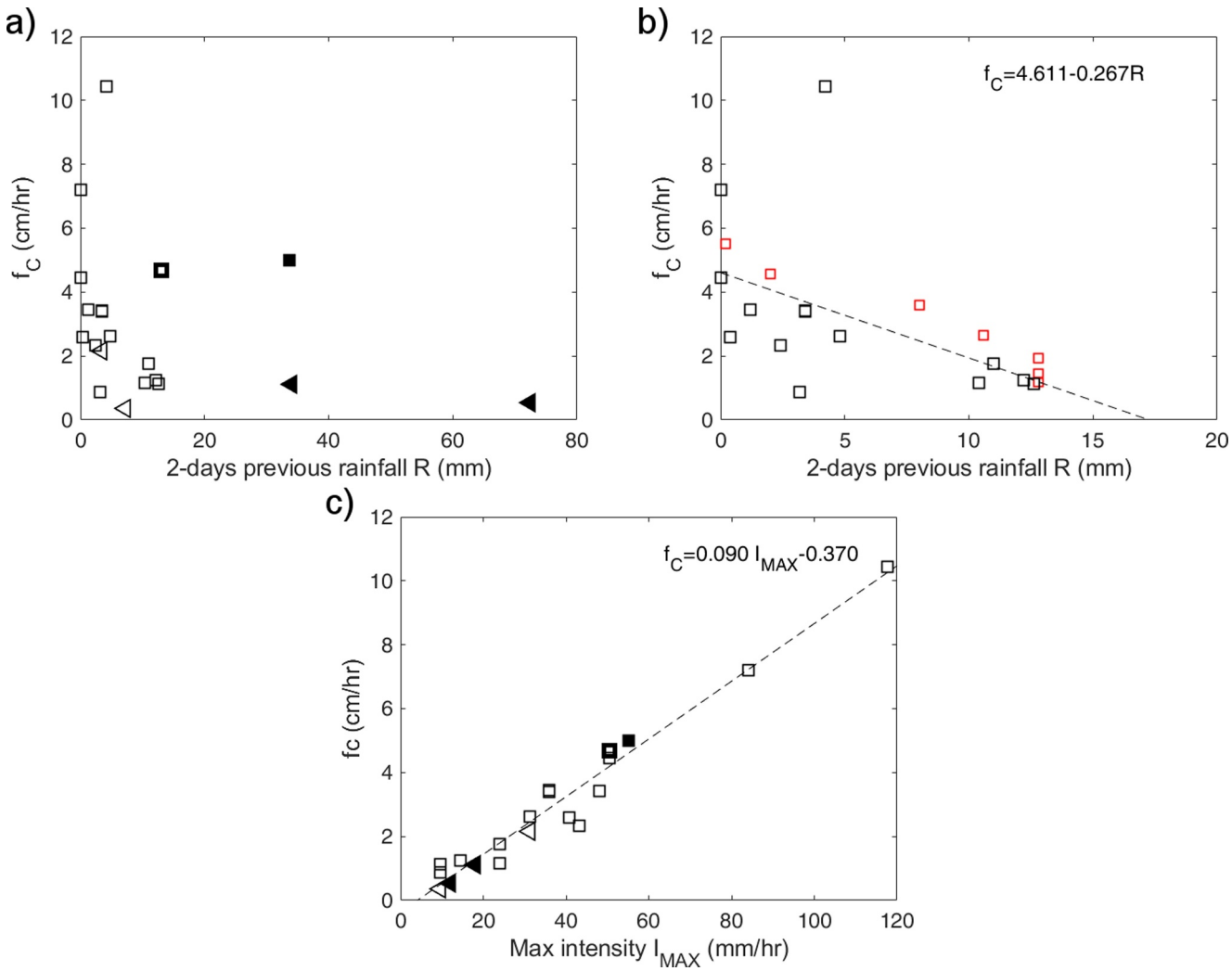

Figure 7. Hortonian infiltration rate, f_C, juxtaposed with the cumulative rainfall from the preceding 2 days. In the figure, squares correspond to the infiltration rates for events detailed in Table 4, while triangles denote events where the weir data is absent, as discussed in Section 3.2. Marker thickness illustrates the AMC of each event, ranging from the thinnest marker for AMC I to the thickest for AMC III. Panel (a) includes all events, whereas panel (b) is specific to AMC I events, showcasing their infiltration rates, f_C. Red squares highlight particular events that experienced no runoff despite the maximum rainfall intensity surpassing the infiltration rate f_C determined by the preceding equation. Panel (c) relates the infiltration rates, f_C, to the 5-min maximum intensity of the associated rainfall events, with an intercept of −0.370 cm/hr and an angular coefficient of 0.090 cm/mm, ascertained solely from these specific events.

We simulate the events using the relationship shown in Figure 7c, reported in Figure 6 to avoid overloading the text. The results show a reasonable reproduction of the observed events, supported by the values of the performance parameter Π_s (Equation 4) detailed in Table 4. In this case as well, the poorest Π_s values result from the simulation of the events that occurred on 25 and 28 June 2017. These events were characterized by long-duration, low-intensity rainfall. In these cases, modeling the excess infiltration using a Hortonian mechanism may not represent the actual runoff generation process.

3.3. Reproducing the Triggering of Debris Flow Events

The refined model, calibrated for the Dimai watershed, was then applied to the monitored catchments of Rio Gere and Rovina di Cancia, comparing: (a) the modeled peak runoff time and the initiation of the debris flows; (b) the shapes of the simulated and recorded stage hydrographs. Since their installation, the monitoring stations in these catchments have witnessed several debris flow events. In the Rovina di Cancia catchment, stage hydrographs were recorded for five of these events: 23 July 2015; 1 August 2018; 1 July 2020; 26 July 2022; 3 July 2023. In the Rio Gere catchment, three events were recorded: on 8 July 2021, 20 July 2023, and 28 August 2023. In the

Table 5
Runoff Events Observed in the Dimai Watershed During Periods When the Sharp-Crested Weir Was Missing

Date	Cumulative rainfall 2 days before (mm)	AMC	f_C (cm/hr)	Required f_C (cm/hr)	Δt (min)
11 July 2010	3.0	1	3.24		−0.6
23 July 2010	6.5	1	2.40		−0.2
04 August 2010	4.2	1	2.95		−0.5
08 August 2010	0.0	1	3.96		−2.0
13 August 2010	7.6	1	2.14		−0.3
16 August 2010	34.0	3		1.12	1.3
27 August 2010	0.0	1	3.96		−2.3
16 June 2011	2.4	1	3.38		−1.6
04 July 2011	5.4	1	2.66		0.7
15 July 2011	3.4	1	3.14	2.16	−5.1
16 July 2011	12.8	1	0.89		0.0
23 July 2011	9.0	1	1.80		6.3
31 July 2011	0.0	1	3.96		3.0
09 June 2013	7.2	1	2.23	0.36	1.5
22 June 2013	0.0	1	3.96		1.2
24 June 2013	72.4	3		0.54	−3.2

Note. The f_C parameter is determined using the relationship shown in Figure 7b. *Required* f_C refers to the infiltration rate necessary to match the timing of the observed runoff, while Δt represents the time discrepancy between the recorded and simulated discharges.

initiation area at Rovina di Cancia, video recordings generally show debris flows with a dense solid-liquid front followed by a more dilute body, while at Rio Gere, they show a hyper-concentrated flow, which may increase its solid concentration further downstream.

Based on the findings presented earlier, the CN_A for rocky surfaces is established at 80.2. Meanwhile, CN values for mountain pine slopes (CN = 61) and scree slopes (CN = 65–70, varying with deposit thickness and texture) are derived from existing literature. The velocity U_S is assumed as 0.7 m/s for rocky paths and 0.1 m/s for other terrains. The coefficient f_c for rocky surfaces is determined using the linear relationship depicted in Figure 7c, while for other land uses, guidelines from Gregoretti et al. (2016) are followed. Additionally, field observations establish outlet section widths for the Rovina di Cancia and Rio Gere channels at $\mathcal{B}_0$ = 8.0 and 5.0 m, respectively.

In Figure 8, we illustrate the hydrological simulations of the events alongside the stage hydrographs obtained from two monitoring stations. Stage measurements were acquired using various sensors, each with distinct advantages and limitations: pressure transducers offer reliable transit timing but might have limited recording duration and susceptibility to damage during events. Video reconstruction provides transit timing accuracy but struggles to precisely determine stage values, particularly at night. Conversely, radar or laser sensors offer continuous stage data and accurate timing but might falter when the flow is turbulent or the surface is irregular. At Rovina di Cancia, a pressure transducer derived stages for the 1 August 2018 event, video reconstruction was employed for debris flows on 23 July 2015, and on 1 July 2020, and a radar distance meter was used for events from 2022 onward. In Rio Gere, laser-level sensors recorded stages. Comparing simulated discharges to recorded stage hydrographs focuses on peak timing and shape alignment. The time lag between simulated runoff peaks and the first surge of observed debris flows typically falls within the range of [−2.5, 1.5] minutes, with a good replication of the stage hydrographs. The event that occurred in Cancia on 3 July 2023 (Figure 8e) shows an excellent correspondence in timing between the simulated hydrograph and the measurements taken. Unlike the other recorded stage hydrographs, the depth values go negative. In fact, the event eroded the channel at the measurement section, thus providing negative stage values.

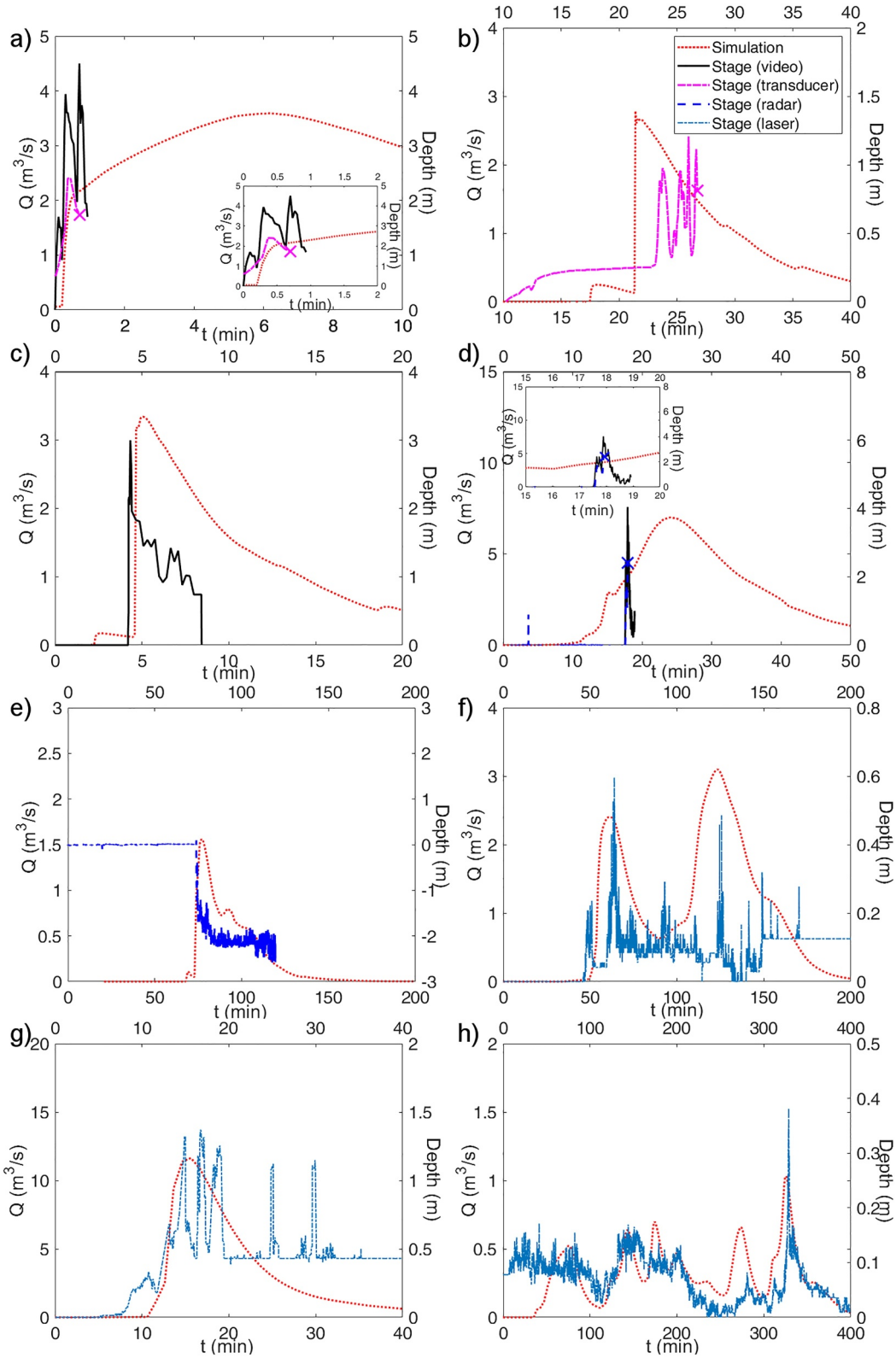

Figure 8. Simulated runoff hydrographs for the rainfall events recorded at Rovina di Cancia (a–e) and Rio Gere (f–h) on: (a) 23 July 2015; (b) 01 August 2018; (c) 01 July 2020; (d) 26 July 2022; (e) 03 July 2023; (f) 08 July 2021; (g) 20 July 2023; (h) 28 August 2023. The values of the parameters adopted in the hydrological model are: $U_S = 0.7$ m/s, $k_S = 9$ m$^{1/3}$/s, and $B_{,} = = 8$ m (Rovina di Cancia), 5 m (Rio Gere). The insert in panels (a) and (d) zooms on the recording of the events.

4. Discussion

The assumption about the CN value adopted in Section 2.3.1 for evaluating the best combination of the I_a coefficient and the number of days for computing the cumulative previous rainfall for determining AMCs was derived from the historical data sets of Gregoretti et al. (2016). However, to validate the analysis performed, we repeated the same analysis, varying the CN values within a range around the initial value (82–95), which is also the range observed in the recorded events (Table 4). We found that the best combination for determining the initial condition of the system remained the same as previously identified, with an average TS = 0.67. This calculation of the parameters for the CN method confirms established knowledge in the literature. Various authors, including Hawkins et al. (2008) and D'Asaro and Grillone (2012), have criticized the proposed initial abstraction $I_a = 0.2S$, emphasizing that this standard value is excessively high in certain contexts, such as alpine environments. Furthermore, alternative methods for assessing AMC, as suggested by Cea and Fraga (2018), have emerged. The different approach to evaluate AMC significantly altered rainfall classification, leading to a notable 70% increase in events categorized as occurring under dry conditions and reductions in those classified as normal or wet. Also Prenner et al. (2018) observed that summer convective phenomena are more frequent over dry soils. This is likely due to the high energy input during the summer season, which leads to high evapotranspiration. The reported CN values, reflective of highly fractured rocky terrains encompassing 95% of the Dimai catchment area, align with those presented by Hawkins et al. (2010), indicating an abrupt increase in CN (termed as a "violent behavior" of the catchment) beyond certain precipitation thresholds, eventually stabilizing at a higher value, CN_∞. In Figure 4, we depict a transversal profile of a rock wall, illustrating different hypothetical paths of surface/subsurface discharges to reach the main channel. Therefore, we highlight mechanisms of faster and slower return, linked to the Hortonian mechanism rather than the saturation excess one. In fact, although the SCS-CN method predicts the total runoff volume of events, it fails to precisely determine peak discharges and hydrograph shapes. This is primarily due to its inability to correctly evaluate the impulsive runoff-contributing rainfall pattern, stemming from its failure to account for the infiltration excess mechanism. Conditions in our study area, characterized by small, steep, bedrock-dominated basins with rapid hydrological responses, contrast sharply with the larger, more moderately sloped basins with diverse land covers where the CN method was originally developed and is more commonly applied. In Dolomitic basins, the dominant bedrock substrate promotes rapid surface runoff, emphasizing the need for hydrological models that can accurately capture these unique characteristics and the predominant Hortonian flow generation processes, as demonstrated by Gregoretti et al. (2016).

The infiltration excess mechanism is considered through the infiltration rate. The variability range for f_C appears compatible with values measured by Li et al. (2011) in dolomite rocky outcrops. These values could be explained by the high degree of fracturing in the Dolomite rock masses (Marchi et al., 2008). The dependence of infiltration rate on the maximum recorded precipitation intensity might seem contradictory; however, it has been widely observed in the past, both in laboratory tests (Morin & Benyamini, 1977; Nassif & Wilson, 1975) and in natural conditions (Yu et al., 1998). This infiltration mechanism, stemming from rock fracturing, resembles the discharge pattern of an orifice, wherein infiltrated flow increases with hydraulic load. Several explanations have been proposed over the years, including the erosion of the seal layer, which is the thin surface layer promoting runoff and reducing infiltration (Valentin, 1993). With higher rainfall intensities (and kinetic energy of raindrops), there is a greater brushing-off effect on the sealing of the soil surface, resulting in higher infiltration rates (Bowyer-Bower, 1993; Morin & Benyamini, 1977). Another explanation involves the formation of a shallow saturated zone in the surface seal layer, leading to a higher hydraulic gradient and higher infiltration (Mualem et al., 1993). In our study area, the most plausible explanation may be related to the high degree of fracturing of rocky outcrops. Li et al. (2011) demonstrated that the presence of cracks in rocky surfaces increases the infiltrated component of rainfall, thereby significantly reducing the runoff coefficient of the tested plots. Moreover, these findings seem to support the limited influence of antecedent moisture conditions on the watershed response in such an environment (Berti et al., 2012; Mostbauer et al., 2018; Wieczorek & Glade, 2005).

Regarding the replication of debris flow hydrograph, we found a small time lag between simulation and observation. This aligns with debris flow initiation mechanisms closely associated with runoff destabilizing in-channel sediment layers. A small lag signifies relatively robust model performance. The simulations generally replicate stage hydrographs well, especially for hyper-concentrated events at Rio Gere. However, for more developed debris flows, the rising limb of simulated hydrographs often matches the abrupt level increase in the channel, while the falling limb shows lower accuracy, with simulated runoff dropping below the critical threshold for debris flow occurrence. Notably, our model struggles to replicate the 26 July 2022 event (Figure 8d), as evidenced

by video footage capturing a fully developed debris flow surge. In this event, the strong liquid current likely transferred significant momentum to the sediment, leading to the formation of a solid-liquid wave and subsequent flow deceleration. However, our findings resonate with those of Rengers et al. (2016, 2019), who, similar to this study, compared model-predicted peak discharge times with stage hydrographs during debris flow events, leading to the conclusion that hydrological models can simulate the initiation time of runoff-generated debris flows. It is important to note that this methodology should be applied to the initiation phase of debris flows when a solid-liquid head forms, followed by a liquid body, that is, before the sediment bulking that transforms the whole wave into a solid-liquid flow. It does not explicitly account for the complex processes governing debris flow initiation and sediment entrainment into the flow that causes the volumetric growth of up to one order of magnitude (Reid et al., 2016; Simoni et al., 2020). Indeed, while traditional hydrological models, including the Curve Number approach, can provide valuable insights into water-dominated flows, they cannot fully represent the unique dynamics of debris flow events when applied to such phenomena. Notably, debris flows exhibit significantly higher peak discharges compared to water flows due to sediment bulking and complex surge dynamics. These surge phenomena, often not directly tied to fluctuations in rainfall intensity (Berti et al., 2000), result from the interaction between water and sediment, leading to pulsating flow behavior that cannot be adequately replicated by standard hydrological models. In fact, in Figure 8d, the proposed model cannot capture the solid-liquid hydrograph of the mature debris flow that occurred on 23 July 2022. In such an event, the debris flow formed in the upper part of the channel, reaching a high solid content upstream of the monitoring section.

The inherent challenges in accurately predicting debris flow phenomena, even with the extensive monitoring and modeling efforts undertaken in this study, must be acknowledged. The present study is among the few (Rengers et al., 2016, 2019; Tang et al., 2019, 2020) using a modeling approach based on experimental data observed in the field. While our study focuses on a specific area in the Dolomites, it is important to emphasize that the methodology we have developed can be adapted and applied more broadly. Our approach demonstrates how to tailor a hydrological model to the particular characteristics of a study area, providing a framework that can be generalized to other geomorphological settings. Researchers studying different environments can adapt this method, modifying the hydrological model to suit their specific area characteristics. For instance, while we combined the SCS-CN method with a simple hortonian infiltration law for our steep, bedrock-dominated basins, other studies like Rengers et al. (2016) have employed different methods, such as the Green-Ampt method for modeling infiltration, which was more suitable for their study site. This adaptable methodology is particularly valuable for predicting the initial phases of debris flows in various environments. By customizing the model to local conditions, more accurate predictions of debris flow initiation across different geological and hydrological contexts can be achieved. However, while our results represent a significant step forward, consistently reliable predictions in such a complex environment remain elusive, especially due to the difficulties related to data collection in the initiation areas, which significantly hinder progress in the field. Furthermore, the physical peculiarities of debris flow catchments demand specific tools that differ significantly from those used in larger basins, where water-dominant flows occur.

In this study, we applied the model to watersheds with a single channel that concentrates and routes surface runoff from the above rock walls through gullies or fractures onto alluvial fans, where it mobilizes the existing debris deposits. However, the model can also be applied to assess catchments with multiple channels in deposits of loose materials, where it is unclear whether only one or several would produce debris flows triggered by a specific precipitation event. This is the case also highlighted in Barbini et al. (2024), where the Rusecco basin (San Vito di Cadore, BL), adjacent to the north of the Rovina di Cancia catchment, was analyzed. In this instance, hydrological modeling was conducted for all the sub-catchments that, according to geomorphological analysis and surveys, could generate debris flows. Most of these were sub-catchments affecting different sediment source areas, while one sub-catchment had multiple channels affecting the same large debris deposit derived from a massive rock failure. In general, prior to applying the model, a study must be conducted to effectively assess the availability of sediment in the basin under investigation, in order to run simulations on potentially affected areas.

The ability of the model to determine the hydrograph shape and peak time indicates its potential utility for early warning systems to predict debris flow occurrences (Bernard & Gregoretti, 2021). It may also aid in calculating the solid-liquid hydrograph necessary for executing models that simulate debris flow propagation. For instance, the runoff contributing to debris flow and the related solid-liquid hydrograph can be identified and modeled following the methods outlined by De Paola et al. (2017) and Barbini et al. (2024). Estimating the volume of sediment that can be mobilized is critical for assessing hazards and risks, designing effective structural

safeguards, and formulating efficient emergency management regulations, as highlighted by Ghilardi et al. (2001). This requires reliable data on sediment transport during debris flow events to evaluate sediment-volume concentration. Once a significant data set is established, detailing the volume balance of mobilized sediments for each event, it becomes possible to estimate the volume of debris flow in the initiation area (Simoni et al., 2020). By comparing this with the modeled discharge, an estimation of the sediment-volume concentration of the initial surge can be obtained. This approach enables a more in-depth analysis of debris flow formation modeling.

5. Conclusions

Monitoring the impervious dynamics of dolomitic headwater catchments poses challenges. Understanding precipitation-runoff relations is essential to enhance our knowledge about debris flow triggering and to model initiation dynamics on scree slopes beneath rocky cliffs. The installation of a sharp-crested weir at the outlet of the Dimai headwater catchment (Cortina d'Ampezzo, BL) provided valuable hydrological data for dolomitic watersheds.

The hydrological response to multiple convective rainfall events was recorded for the catchment in the period 2010–2017. Hydrographs exhibit an impulsive nature, reminiscent of debris flow stage hydrographs, with a rapid decrease in discharge, stabilizing at a near-constant level. This runoff pattern aligns with observations by Gregoretti et al. (2016) and can be represented by two rectangular stages: an initial tall, narrow peak followed by a shorter, prolonged one.

Initial hydrological modeling conducted demonstrated that, although the SCS-CN method can predict the total runoff volume of events, it falls short in determining peak discharges and hydrograph shapes. This shortcoming arises mainly from its inability to correctly evaluate the impulsive runoff-contributing rainfall pattern, as it does not account for the infiltration excess mechanism.

To address these issues, we adopted the model suggested by Gregoretti et al. (2016), modifying the method for calculating excess infiltration for a closer match with experimental data. The *CN* coefficients, fine-tuned to ensure alignment between observed and simulated runoff volumes, vary slightly, averaging around 80.2. This model replicates the peak-discharge value and timing, as well as the total runoff volume. The comparison between our simulation and available evidence indicates that the key element to achieving a good match is the relationship that connects the infiltration rate to the maximum rainfall intensity: the higher the precipitation intensity, the greater the infiltrated part.

To test the robustness of the model and validate its predictions, we take advantage of more field monitoring data collected from two larger debris flow prone catchments located in the same Dolomite area. Specifically, we compare the simulated runoff with the timing and shaping of seven events that occurred in the Rio Gere and Rovina di Cancia catchments in response to extreme rainfalls. The proposed model reproduces the timing of the peak discharge observed in the initiation area of the two catchments. Differences in timing are only a few minutes, ensuring acceptable accuracy of the model. Additionally, the shape of the stage hydrographs seems to be adequately replicated. However, available data indicate that the fit is more satisfactory in the case of hyper-concentrated flows not yet fully developed as debris flows. Whenever a mature debris flow surge is observed, the curbing effect of the coarse-grained granular snout introduces some delay in the downslope propagation of the phenomena; therefore, our predictions tend to anticipate the actual flow stage growth and peak discharge.

The model exhibits promise in predicting runoff shape and peak time, which are relevant factors for hazard management. It can provide input hydrographs for debris flow routing models, potentially improving their accuracy. These capabilities suggest two potential applications. First, the model could be used to forecast debris flow occurrences based on rainfall data, offering a tool for early warning systems (Bernard & Gregoretti, 2021). Second, it might aid in hazard assessment, design of protective structures, and emergency management protocols by estimating mobilizable sediment volume. However, accurately determining solid-volume concentrations within debris flows requires complex sediment budget analysis after each event. The need for such data underscores the importance of further research in this area, which will be addressed in a future study.

Data Availability Statement

Video mentioned in Section 3.3 are available in Bernard et al. (2024).

Acknowledgments

This study was carried out within the RETURN Extended Partnership and received funding from the European Union Next-GenerationEU (National Recovery and Resilience Plan—NRRP, Mission 4, Component 2, Investment 1.3—D.D. 1243 2/8/2022, PE0000005). It was also supported by the following projects: "RESILIENCE (Extreme Storms in the Italian North-East: frequency, impacts and projected changes)," funded by CARIPARO foundation; "INADEF (Innovative eArly warning system for Debris Flow)" funded by the Interregional program Italy-Austria of European Union; "GAPDEMM (GIS-based integrated platform for Debris Flow Monitoring, Modeling and Hazard Mitigation)," funded by CARIPARO foundation; "PARAmount (imProved Accessibility: Reliability and security of Alpine transport infrastructure related to mountainous hazards in a changing climate)" funded by Alpine Space programme of European Union; "Study of new early warning systems against hydrogeological risk and their social perception in a high valuable area for tourism and environment" funded by the University of Padova (CPDA119318); "Forecasting of hazardous mass movement phenomena in the current climate change" funded by the Italian Ministry of Education, University and Research. The authors would like to thank the association "Regole d'Ampezzo" for permitting the setup of the experimental facilities in Dimai and Rio Gere. They would also like to express their gratitude to the association "Regola di Borca di Cadore" for granting authorization to monitor the Rovina di Cancia catchment. Special thanks go to the Department of Land Defense and Civil Protection of the Province of Belluno for permitting the setup of the experimental facilities in Rovina di Cancia, providing LiDAR data sets, and supplying data from the upper rain gauge at Cancia. The Environmental Protection Agency of the Veneto Region is acknowledged for providing data from the stand-alone rain gauges in Rovina di Cancia and Son Forca. Lastly, the authors would like to extend their thanks to Massimo Degetto, Giacomo Crucil, Alessandro Pimazzoni, and Gianpiero De Vido for their assistance in the field.

References

Bacchini, M., & Zannoni, A. (2003). Relations between rainfall and triggering of debris-flow: Case study of Cancia (Dolomites, northeastern Italy). *Natural Hazards and Earth System Sciences*, *3*(1/2), 71–79. https://doi.org/10.5194/nhess-3-71-2003

Baggio, T., Mergili, M., & D'Agostino, V. (2021). Advances in the simulation of debris flow erosion: The case study of the Rio Gere (Italy) event of the 4th August 2017. *Geomorphology*, *381*, 107664. https://doi.org/10.1016/j.geomorph.2021.107664

Barbini, M., Bernard, M., Boreggio, M., Schiavo, M., D'Agostino, V., & Gregoretti, C. (2024). An alternative approach for the sediment control of in-channel stony debris flows with an application to the case study of Ru Secco Creek (Venetian Dolomites, Northeast Italy). *Frontiers in Earth Science*, *12*. https://doi.org/10.3389/feart.2024.1340561

Bernard, M. (2018). Analysis and modelling of surface runoff triggering debris flows (Doctoral Thesis). *Università degli Studi di Padova*.

Bernard, M., Barbini, M., Berti, M., Simoni, A., Boreggio, M., & Gregoretti, C. (2024). Data of rainfall-runoff modelling in rocky headwater catchments for the prediction of debris flow occurrence [Video]. Retrieved from https://www.hydroshare.org/resource/1f62186d1bf64bc2aacc46f231622b23/

Bernard, M., Berti, M., Simoni, A., & Gregoretti, C. (2019). Characteristics of debris flows just downstream the initiation area on Punta Nera cliffs, Venetian Dolomites. In J. W. Kean, J. A. Coe, P. M. Santi, & B. K. Guillen (Eds.), *Debris-flow hazards mitigation: Mechanics, monitoring, modeling, and assessment*. Association of Environmental and Engineering Geologists.

Bernard, M., Boreggio, M., Degetto, M., & Gregoretti, C. (2019). Model-based approach for design and performance evaluation of works controlling stony debris flows with an application to a case study at Rovina di Cancia (Venetian Dolomites, Northeast Italy). *Science of the Total Environment*, *688*, 1373–1388. https://doi.org/10.1016/j.scitotenv.2019.05.468

Bernard, M., & Gregoretti, C. (2021). The use of rain gauge measurements and radar data for the model-based prediction of runoff-generated debris-flow occurrence in early warning systems. *Water Resources Research*, *57*(3), 2020WR027893. https://doi.org/10.1029/2020WR027893

Berti, M., Bernard, M., Simoni, A., & Gregoretti, C. (2020). Physical interpretation of rainfall thresholds for runoff-generated debris flows. *Journal of Geophysical Research: Earth Surface*, *125*(6), e2019JF005513. https://doi.org/10.1029/2019JF005513

Berti, M., Genevois, R., LaHusen, R. G., Simoni, A., & Tecca, P. R. (2000). Debris flow monitoring in the Acquabona watershed on the Dolomites (Italian Alps). *Physics and Chemistry of the Earth - Part B: Hydrology, Oceans and Atmosphere*, *25*(9), 707–715. https://doi.org/10.1016/S1464-1909(00)00090-3

Berti, M., Genevois, R., Simoni, A., & Tecca, P. R. (1999). Field observations of a debris flow event in the Dolomites. *Geomorphology*, *29*(3–4), 265–274. https://doi.org/10.1016/S0169-555X(99)00018-5

Berti, M., Martina, M. L. V., Franceschini, S., Pignone, S., Simoni, A., & Pizziolo, M. (2012). Probabilistic rainfall thresholds for landslide occurrence using a Bayesian approach. *Journal of Geophysical Research*, *117*(F4), F04006. https://doi.org/10.1029/2012JF002367

Berti, M., & Simoni, A. (2005). Experimental evidences and numerical modelling of debris flow initiated by channel runoff. *Landslides*, *2*(3), 171–182. https://doi.org/10.1007/s10346-005-0062-4

Beven, K. J. (2002). Runoff generation in semi-arid areas. In L. Bull, & M. J. Kirkby (Eds.), *Dryland rivers: Hydrology and geomorphology of semi-arid channels* (pp. 57–105). Wiley.

Bollschweiler, M., & Stoffel, M. (2010). Changes and trends in debris-flow frequency since AD 1850: Results from the Swiss Alps. *The Holocene*, *20*(6), 907–916. https://doi.org/10.1177/0959683610365942

Boreggio, M., Bernard, M., & Gregoretti, C. (2022). Does the topographic data source truly influence the routing modelling of debris flows in a torrent catchment? *Earth Surface Processes and Landforms*, *47*, 1–23. https://doi.org/10.1002/esp.5366

Bouvier, C., Brunet, P., Le Bourgeois, O., Nguyen, S., Borrell, V., Ayral, P.-A., et al. (2015). Hydrological processes generating flash floods at hillslope scale in a small mountainous Mediterranean catchment. *EGU General Assembly*, 2015.

Bowyer-Bower, T. A. S. (1993). Effects of rainfall intensity and antecedent moisture on the steady-state infiltration rate in a semi-arid region. *Soil Use & Management*, *9*(2), 69–75. https://doi.org/10.1111/j.1475-2743.1993.tb00932.x

Brayshaw, D., & Hassan, M. A. (2009). Debris flow initiation and sediment recharge in gullies. *Geomorphology*, *109*(3–4), 122–131. https://doi.org/10.1016/j.geomorph.2009.02.021

Cannon, S. H., Gartner, J. E., Rupert, M. G., Michael, J. A., Rea, A. H., & Parrett, C. (2010). Predicting the probability and volume of postwildfire debris flows in the intermountain western United States. *Geological Society of America Bulletin*, *122*(1–2), 127–144. https://doi.org/10.1130/B26459.1

Cannon, S. H., Gartner, J. E., Wilson, R. C., Bowers, J. C., & Laber, J. L. (2008). Storm rainfall conditions for floods and debris flows from recently burned areas in southwestern Colorado and southern California. *Geomorphology*, *96*(3–4), 250–269. https://doi.org/10.1016/j.geomorph.2007.03.019

Cea, L., & Fraga, I. (2018). Incorporating antecedent moisture conditions and intraevent variability of rainfall on flood frequency analysis in poorly gauged basins. *Water Resources Research*, *54*(11), 1–18. https://doi.org/10.1029/2018WR023194

Chow, V. T., Maidment, D. R., & Mays, L. W. (1988). *Applied hydrology*. McGraw-Hill.

Coe, J. A., & Godt, J. W. (2003). Estimating debris-flow probability using fan stratigraphy, historic records, and drainage-basin morphology. Interstate 70 highway corridor, central Colorado, U.S.A. *Debris-Flow Hazards Mitigation: Mechanics, Prediction, and Assessment*, 1085–1096.

Coe, J. A., Kinner, D. A., & Godt, J. W. (2008). Initiation conditions for debris flows generated by runoff at Chalk Cliffs, central Colorado. *Geomorphology*, *96*(3–4), 270–297. https://doi.org/10.1016/j.geomorph.2007.03.017

Damm, B., & Felderer, A. (2013). Impact of atmospheric warming on permafrost degradation and debris flow initiation—A case study from the eastern European Alps. *EG Quaternary Science Journal*, *62*(2), 136–149. https://doi.org/10.3285/eg.62.2.05

D'Asaro, F., & Grillone, G. (2012). Empirical investigation of curve number method parameters in the Mediterranean area. *Journal of Hydrologic Engineering*, *17*(10), 1141–1152. https://doi.org/10.1061/(ASCE)HE.1943-5584.0000570

Degetto, M., Gregoretti, C., & Bernard, M. (2015). Comparative analysis of the differences between using LiDAR and contour-based DEMs for hydrological modeling of runoff generating debris flows in the Dolomites. *Frontiers in Earth Science*, *3*, 1–15. https://doi.org/10.3389/feart.2015.00021

de Haas, T., Lau, C.-A., & Ventra, D. (2024). Debris-flow watersheds and fans: Morphology, sedimentology and dynamics. In *Advances in debris-flow science and practice* (pp. 9–73). Springer International Publishing. https://doi.org/10.1007/978-3-031-48691-3_2

De Paola, F., De Risi, R., Di Crescenzo, G., Giugni, M., Santo, A., & Speranza, G. (2017). Probabilistic assessment of debris flow peak discharge by Monte Carlo simulation. *ASCE-ASME Journal of Risk and Uncertainty in Engineering Systems, Part A: Civil Engineering*, *3*(1), A4015002. https://doi.org/10.1061/AJRUA6.0000855

Draebing, D., & Krautblatter, M. (2019). The efficacy of frost weathering process in alpine rockwalls. *Geophysical Research Letters*, *46*(12), 6516–6524. https://doi.org/10.1029/2019GL081981

Floris, M., D'Alpaos, A., Squarzoni, C., Genevois, R., & Marani, M. (2010). Recent changes in rainfall characteristics and their influence on thresholds for debris flow triggering in the Dolomitic area of Cortina d'Ampezzo, north-eastern Italian Alps. *Natural Hazards and Earth System Sciences*, *10*(3), 571–580. https://doi.org/10.5194/nhess-10-571-2010

Foglia, L., Hill, M. C., Mehl, S. W., & Burlando, P. (2009). Sensitivity analysis, calibration, and testing of a distributed hydrological model using error-based weighting and one objective function. *Water Resources Research*, *45*(6), 1–18. https://doi.org/10.1029/2008WR007255

Fuchs, S., Heiss, K., & Hübl, J. (2007). Towards an empirical vulnerability function for use in debris flow risk assessment. *Natural Hazards and Earth System Sciences*, *7*(5), 495–506. https://doi.org/10.5194/nhess-7-495-2007

Gatter, R., Cavalli, M., Crema, S., & Bossi, G. (2018). Modelling the dynamics of a large rock landslide in the Dolomites (eastern Italian Alps) using multi-temporal DEMs. *PeerJ*, *6*, e5903. https://doi.org/10.7717/peerj.5903

Ghilardi, P., Natale, L., & Savi, F. (2001). Modeling debris flow propagation and deposition. *Physics and Chemistry of the Earth—Part C: Solar, Terrestrial & Planetary Science*, *26*(9), 651–656. https://doi.org/10.1016/S1464-1917(01)00063-0

Gregoretti, C., & Dalla Fontana, G. (2007). Rainfall threshold for the initiation of debris flows by channel-bed failure in the Dolomites. In C. Chen, & J. J. Major (Eds.), *Debris-flow mitigation: Mechanics, prediction and assessment* (pp. 11–21). Milpress.

Gregoretti, C., Degetto, M., Bernard, M., & Boreggio, M. (2018). The debris flow occurred at Ru Secco Creek, Venetian Dolomites, on 4 August 2015: Analysis of the phenomenon, its characteristics and reproduction by models. *Frontiers in Earth Science*, *6*(80), 80. https://doi.org/10.3389/feart.2018.00080

Gregoretti, C., Degetto, M., Bernard, M., Crucil, G., Pimazzoni, A., De Vido, G., et al. (2016). Runoff of small rocky headwater catchments: Field observations and hydrological modeling. *Water Resources Research*, *52*(10), 8138–8158. https://doi.org/10.1002/2016WR018675

Han, X., Chen, J., Xu, P., & Zhan, J. (2017). A well-balanced numerical scheme for debris flow run-out prediction in Xiaojia Gully considering different hydrological designs. *Landslides*, *14*, 1–10. https://doi.org/10.1007/s10346-017-0850-7

R. H. Hawkins, T. J. Ward, D. E. Woodward, & J. A. Van Mullem (Eds.) (2008). *Curve number hydrology*. American Society of Civil Engineers. https://doi.org/10.1061/9780784410042

Hawkins, R. H., Ward, T. J., Woodward, E., & Van Mullem, J. A. (2010). Continuing evolution of rainfall-runoff and the curve number precedent. In *2nd joint federal interagency conference* (pp. 2–12).

Hürlimann, M., Abancó, C., Moya, J., & Vilajosana, I. (2014). Results and experiences gathered at the Rebaixader debris-flow monitoring site, Central Pyrenees, Spain. *Landslides*, *11*(6), 939–953. https://doi.org/10.1007/s10346-013-0452-y

Hürlimann, M., Copons, R., & Altimir, J. (2006). Detailed debris flow hazard assessment in Andorra: A multidisciplinary approach. *Geomorphology*, *78*(3–4), 359–372. https://doi.org/10.1016/j.geomorph.2006.02.003

Imaizumi, F., Sidle, R. C., Tsuchiya, S., & Ohsaka, O. (2006). Hydrogeomorphic processes in a steep debris flow initiation zone. *Geophysical Research Letters*, *33*(10), 2–5. https://doi.org/10.1029/2006GL026250

Jakob, M., & Hungr, O. (2005). *Debris-flow hazards and related phenomena*. Springer Berlin Heidelberg. https://doi.org/10.1007/b138657

Kean, J. W., Staley, D. M., Leeper, R. J., Schmidt, K. M., & Gartner, J. E. (2012). A low-cost method to measure the timing of postfire flash floods and debris flows relative to rainfall. *Water Resources Research*, *48*(5), W05516. https://doi.org/10.1029/2011WR011460

Lanzoni, S., Gregoretti, C., & Stancanelli, L. M. (2017). Coarse-grained debris flow dynamics on erodible beds. *Journal of Geophysical Research: Earth Surface*, *122*(3), 592–614. https://doi.org/10.1002/2016JF004046

Li, X. Y., Contreras, S., Solé-Benet, A., Cantón, Y., Domingo, F., Lázaro, R., et al. (2011). Controls of infiltration-runoff processes in Mediterranean karst rangelands in SE Spain. *Catena*, *86*(2), 98–109. https://doi.org/10.1016/j.catena.2011.03.003

Marchi, L., Dalla Fontana, G., Cavalli, M., & Tagliavini, F. (2008). Rocky headwaters in the Dolomites, Italy: Field observations and topographic analysis. *Artic, Antartic, and Alpine Research*, *40*(4), 685–694. https://doi.org/10.1657/1523-0430(07-037)

Moody, J. A., Martin, D. A., Haire, S. L., & Kinner, D. A. (2008). Linking runoff response to burn severity after a wildfire. *Hydrological Processes*, *22*(13), 2063–2074. https://doi.org/10.1002/hyp.6806

Morin, J., & Benyamini, Y. (1977). Rainfall infiltration into bare soils. *Water Resources Research*, *13*(5), 813–817. https://doi.org/10.1029/WR013i005p00813

Mostbauer, K., Kaitna, R., Prenner, D., & Hrachowitz, M. (2018). The temporally varying roles of rainfall, snowmelt and soil moisture for debris flow initiation in a snow-dominated system. *Hydrology and Earth System Sciences*, *22*(6), 3493–3513. https://doi.org/10.5194/hess-22-3493-2018

Mualem, Y., Assouline, S., & Eltahan, D. (1993). Effect of rainfall-induced soil seals on soil water regime: Wetting processes. *Water Resources Research*, *29*(6), 1651–1659. https://doi.org/10.1029/93WR00096

Musumeci, R. E., Foti, E., Li Rosi, D., Sanfilippo, M., Stancanelli, L. M., Iuppa, C., et al. (2021). Debris-flow hazard assessment at the archaeological UNESCO world heritage site of Villa Romana del Casale (Sicily, Italy). *International Journal of Disaster Risk Reduction*, *64*, 102509. https://doi.org/10.1016/j.ijdrr.2021.102509

Nassif, S. H., & Wilson, E. M. (1975). The influence of slope and rain intensity on runoff and infiltration. *Hydrological Sciences Bulletin*, *20*(4), 539–553. https://doi.org/10.1080/02626667509491586

Okano, K., Suwa, H., & Kanno, T. (2012). Characterization of debris flows by rainstorm condition at a torrent on the Mount Yakedake volcano, Japan. *Geomorphology*, *136*(1), 88–94. https://doi.org/10.1016/j.geomorph.2011.04.006

Orlandini, S., & Rosso, R. (1996). Diffusion wave modeling of distributed catchment dynamics. *Journal of Hydrologic Engineering*, *1*(3), 103–113. https://doi.org/10.1061/(ASCE)1084-0699(1996)1:3(103)

Prenner, D., Hrachowitz, M., & Kaitna, R. (2019). Trigger characteristics of torrential flows from high to low alpine regions in Austria. *Science of the Total Environment*, *658*, 958–972. https://doi.org/10.1016/j.scitotenv.2018.12.206

Prenner, D., Kaitna, R., Mostbauer, K., & Hrachowitz, M. (2018). The value of using multiple hydrometeorological variables to predict temporal debris flow susceptibility in an alpine environment. *Water Resources Research*, *54*(9), 1–22. https://doi.org/10.1029/2018WR022985

Pudasaini, S. P., & Mergili, M. (2019). A multi-phase mass flow model. *Journal of Geophysical Research: Earth Surface*, *124*(12), 2920–2942. https://doi.org/10.1029/2019JF005204

Reid, M. E., Coe, J. A., & Brien, D. L. (2016). Forecasting inundation from debris flows that grow volumetrically during travel, with application to the Oregon Coast Range, USA. *Geomorphology*, *273*, 396–411. https://doi.org/10.1016/j.geomorph.2016.07.039

Rengers, F. K., Kean, J. W., Reitman, N. G., Smith, J. B., Coe, J. A., & McGuire, L. A. (2020). The influence of frost weathering on debris flow sediment supply in an alpine basin. *Journal of Geophysical Research: Earth Surface*, *125*(8), 6041–6061. https://doi.org/10.1029/2019JF005369

Rengers, F. K., McGuire, L. A., Kean, J. W., Staley, D. M., & Hobley, D. E. J. (2016). Model simulations of flood and debris flow timing in steep catchments after wildfire. *Water Resources Research*, *52*(8), 6041–6061. https://doi.org/10.1002/2015WR018176

Rengers, F. K., McGuire, L. A., Kean, J. W., Staley, D. M., & Youberg, A. M. (2019). Progress in simplifying hydrologic model parameterization for broad applications to post-wildfire flooding and debris-flow hazards. *Earth Surface Processes and Landforms*, *44*(15), 3078–3092. https://doi.org/10.1002/esp.4697

Rickenmann, D., Laigle, D., McArdell, B. W., & Hübl, J. (2006). Comparison of 2D debris-flow simulation models with field events. *Computational Geosciences*, *10*(2), 241–264. https://doi.org/10.1007/s10596-005-9021-3

Schaefer, J. T. (1990). The critical success index as an indicator of warning skill. *Weather and Forecasting*, *5*(4), 570–575. https://doi.org/10.1175/1520-0434(1990)005⟨0570:TCSIAA⟩2.0.CO;2

Schulz, K., Beven, K. J., & Huwe, B. (1999). Equifinality and the problem of robust calibration in nitrogen budget simulations. *Soil Science Society of America Journal*, *63*(6), 1934–1941. https://doi.org/10.2136/sssaj1999.6361934x

Sheridan, G. J., Lane, P. N., & Noske, P. J. (2007). Quantification of hillslope runoff and erosion processes before and after wildfire in a wet Eucalyptus forest. *Journal of Hydrology*, *343*(1–2), 12–28. https://doi.org/10.1016/j.jhydrol.2007.06.005

Simoni, A., Bernard, M., Berti, M., Boreggio, M., Lanzoni, S., Stancanelli, L. M., & Gregoretti, C. (2020). Runoff-generated debris flows: Observation of initiation conditions and erosion–deposition dynamics along the channel at Cancia (eastern Italian Alps). *Earth Surface Processes and Landforms*, *45*(14), 3556–3571. https://doi.org/10.1002/esp.4981

Soil Conservation Service. (1972). *National engineering handbook (NEH4) (Technical Report)*. U.S. Department of Agriculture.

Staley, D. M., Kean, J. W., Cannon, S. H., Schmidt, K. M., & Laber, J. L. (2013). Objective definition of rainfall intensity-duration thresholds for the initiation of post-fire debris flows in southern California. *Landslides*, *10*(5), 547–562. https://doi.org/10.1007/s10346-012-0341-9

Stoffel, M., Tiranti, D., & Huggel, C. (2014). Climate change impacts on mass movements—Case studies from the European Alps. *Science of the Total Environment*, *493*, 1255–1266. https://doi.org/10.1016/j.scitotenv.2014.02.102

Takahashi, T. (2014). *Debris flow: Mechanics, prediction and countermeasures* (2nd ed.). CRC Press. https://doi.org/10.1201/b16647

Tang, H., McGuire, L. A., Kean, J. W., & Smith, J. B. (2020). The impact of sediment supply on the initiation and magnitude of runoff-generated debris flows. *Geophysical Research Letters*, *47*(14), e2020GL087643. https://doi.org/10.1029/2020GL087643

Tang, H., McGuire, L. A., Rengers, F. K., Kean, J. W., Staley, D. M., & Smith, J. B. (2019). Evolution of debris-flow initiation mechanisms and sediment sources during a sequence of postwildfire rainstorms. *Journal of Geophysical Research: Earth Surface*, *124*(6), 1572–1595. https://doi.org/10.1029/2018JF004837

Tao, J., & Barros, A. P. (2014). Coupled prediction of flood response and debris flow initiation during warm- and cold-season events in the Southern Appalachians, USA. *Hydrology and Earth System Sciences*, *18*(1), 367–388. https://doi.org/10.5194/hess-18-367-2014

Theule, J. I., Liébault, F., Loye, a., Laigle, D., & Jaboyedoff, M. (2012). Sediment budget monitoring of debris-flow and bedload transport in the Manival Torrent, SE France. *Natural Hazards and Earth System Sciences*, *12*(3), 731–749. https://doi.org/10.5194/nhess-12-731-2012

Thiene, M., Shaw, W. D., & Scarpa, R. (2017). Perceived risks of mountain landslides in Italy: Stated choices for subjective risk reductions. *Landslides*, *14*(3), 1077–1089. https://doi.org/10.1007/s10346-016-0741-3

Tiranti, D., & Deangeli, C. (2015). Modeling of debris flow depositional patterns according to the catchment and sediment source area characteristics. *Frontiers in Earth Science*, *3*, 1–14. https://doi.org/10.3389/feart.2015.00008

Underwood, S. J., Schultz, M. D., Berti, M., Gregoretti, C., Simoni, A., Mote, T. L., & Saylor, A. M. (2016). Atmospheric circulation patterns, cloud-to-ground lightning, and locally intense convective rainfall associated with debris flow initiation in the Dolomite Alps of northeastern Italy. *Natural Hazards and Earth System Sciences*, *16*(2), 509–528. https://doi.org/10.5194/nhess-16-509-2016

Valentin, C. (1993). Soil crusting and sealing in West Africa and possible approaches to improved management. In *Soil tillage in Africa: Needs and challenges (chapter 9)*. Food and Agriculture Organization of the United Nations.

Wei, Z., Shang, Y., Zhao, Y., Pan, P., & Jiang, Y. (2017). Rainfall threshold for initiation of channelized debris flows in a small catchment based on in-site measurement. *Engineering Geology*, *217*, 23–34. https://doi.org/10.1016/j.enggeo.2016.12.003

Wieczorek, G. F., & Glade, T. (2005). Climatic factors influencing occurrence of debris flows. In *Debris-flow hazards and related phenomena* (pp. 325–362). Springer Berlin Heidelberg. https://doi.org/10.1007/3-540-27129-5{_}14

Yu, B., Cakurs, U., & Rose, C. W. (1998). An assessment of methods for estimating runoff rates at the plot scale. *Transactions of the ASAE*, *41*(3), 653–661. https://doi.org/10.13031/2013.17233

Zimmermann, M., Mani, P., & Romang, H. (1997). Magnitude-frequency aspects of alpine debris flows. *Eclogae Geologicae Helvetiae*, *90*(3), 415–420. https://doi.org/10.5169/seals-168173